April 2019

GYROSCOPIC STABILIZATION FOR UNIAXIAL HAND TREMORS

Alec Stefan Wehse
Worcester Polytechnic Institute

David Muse
Worcester Polytechnic Institute

Ian Sun
Worcester Polytechnic Institute

Follow this and additional works at: https://digitalcommons.wpi.edu/mqp-all

GYROSCOPIC STABILIZATION FOR UNIAXIAL ROTATIONAL HAND TREMORS

A Major Qualifying Project submitted to the faculty of

Worcester Polytechnic Institute

In partial fulfilment of the requirements for the

Degree of Bachelor of Science in Mechanical Engineering

Submitted by:

_____   _____   _____

David Muse   Ian Sun   Alec Wehse

Project Advisors:

_____   _____

Professor David Planchard   Professor John Hall

April, 2019

ABSTRACT

The goal of this project was to create a device to reduce the magnitude of hand tremors in individuals with Parkinson's disease or Essential Tremor. We focused primarily on tremors that caused the hand to rotate about a central oscillator parallel to the forearm. We utilized the physical properties of a spinning gyroscope to act as the stabilization mechanism and dampen the tremor effects experienced by the individual. Our final prototype uses a small electric motor to spin a gyroscope on a swinging cradle. This allows for natural precession of the gyroscope due to an input torque and generates a counter torque along the axis of the hand's rotation. To monitor the device, we incorporated an RPM sensor in conjunction with an Arduino to receive sensory information about the gyroscope. Through testing, the device achieved an 83% reduction in tremor amplitude.

EXECUTIVE SUMMARY

The major goal of this project was to create a device that reduces the magnitude of hand tremors in individuals with Parkinson's disease or Essential Tremor. At the beginning of the project, the team created design goals to set optimal parameters to strive for. Included in these specifications was to eliminate hand tremors by 70%, while keeping the device under 1 lb. and comfortable for the user. The design of each of the components went through several design iterations and rounds of prototyping, resulting in a single final design. Along with the design of these components, a mathematical model was also developed to describe the forces acting within the system. This aided the team's overall design and demonstrates potential to improve the device.

To develop a mathematical model, the team based some of the work on a thesis paper from Brigham Young University that described the forces at work for a theoretical gyroscopic stabilizer acting on a hand tremor. By summing the torque vectors of the hand, system, and those created by the gyroscope, the model generates an overall torque vector. With different input conditions including RPM and hand rotation, the model showed a theoretical maximum tremor reduction of up to 87%.

At the heart of the device is the gyroscope and driving motor. The gyroscope is a cylindrical brass piece that fits over the motor. This is to both allow for the highest possible angular momentum as well as allow the motor to sit within the gyroscope to make the system more compact. The motor is a small DC electric motor that can spin the gyroscope from 4,400 RPM to a maximum of 26,400 RPM to give the gyroscope a range of angular momentums.

The body and cradle hold the motor and gyroscope assembly while also allowing the gyroscope to precess along a single axis perpendicular to the oscillatory motion of the tremor.

This precession generates a counter torque due to the tremor input torque and thereby creates the gyroscopic stabilization.

Using a model of a hand, the team was able to create an ergonomic mount for the device. By extruding the bottom of the test mount attachment to the surface of the hand, the team created an ergonomic surface to match the surface geometry of an average adult male's hand. The method of creation makes it easily customizable for 95% of hands.

The electrical system provides power and control over the speed at which the gyroscope spins. Using a lithium polymer battery for maximum power output, the speed of the gyroscope is controlled by a speed controller in conjunction with a servo tester. To monitor RPM, an RPM sensor is installed in the cradle and is wired to an Arduino for data processing.

To test the effectiveness of the device, the team developed and conducted a lever arm test. The test operates by mounting the device to the end of a lever arm and measuring the swing times across different angular displacements and different RPMs. Based on this testing, the device was capable of reducing the motion of the lever arm by up to 83%.

ACKNOWLEDGEMENTS

TABLE OF CONTENTS

TABLE OF FIGURES

TABLE OF TABLES

NOMENCLATURE

Symbol	Definition	Units
m_f	Mass of Gyroscope	g
m_w	Mass of Hand	g
D	Distance	mm
r_f	COM of Gyroscope Along Y Axis	mm
x_p	Center of Precession Axis Along X1	mm
y_p	Center of Precession Axis Along Y1	mm
t	Time	$Seconds\ (s)$
f	Frequency	$Hertz$
Φ	Angular Displacement About the Precession Axis	deg
Ω	Angular Velocity of the Gyroscope	RPM
ω	Angular Velocity about the Wrist Joint	deg/s
φ	Angular Velocity about the Precession Axis	deg/s
q	Angular Displacement Matrix	deg
q_{acc}	Angular Acceleration Matrix	deg/s^2
$T_{w.in}$	Torque	$N*mm$
$T_{w.r}$	Reaction torque caused by the system	$N*mm$
T_p	Torque generated about the precession axis	$N*mm$
T	Net torque in the System	$N*mm$
I_{xf}	Gyroscope Moment of Inertia About the X	$g*mm^2$
I_{yf}	Gyroscope Moment of Inertia about the Y	$g*mm^2$
I_{zf}	Gyroscope Moment of Inertia about the Z	$g*mm^2$
I_{zs}	Moment of Inertia of the Assembly about Z1	$g*mm^2$
L	Angular Momentum	$g*mm^2/s$

1.0 INTRODUCTION

Hand tremors are a condition that impact approximately 7 million people in the United States each year and are caused by a number of underlying conditions. The severity of hand tremors ranges from being a mild irritation to a large disability that dramatically impacts people's daily lives. Activities like eating, dressing, chores, etc., all become sufficiently more difficult with the inability to keep one's arms and hands steady. In order to improve the quality of life for individuals with these conditions, it is imperative to find ways to reduce and eliminate hand tremors.

Due to the fact that there are several underlying conditions that cause hand tremors, there is no single solution that is effective. As previously stated, hand tremors can stem from many different origins within the body. The most common of these are Parkinson's Disease and Essential Tremor. Parkinson's Disease, along with other symptoms, limits the brain's ability to create dopamine, which in turn manifests as a tremor. Essential Tremor is a disorder that is not yet fully understood. It has been observed to be passed down genetically and causes individuals to have tremors in various locations and severities. The current treatments for these conditions, such as beta-blockers for Essential Tremor and Levodopa for Parkinson's can be effective, however they are not permanent solutions. To help alleviate the impact of tremors, there have been a number of devices and products made to either reduce the effect of the tremor during a specific activity, or to reduce the tremor entirely.

These devices can be very helpful in allowing people with hand tremors complete everyday tasks that would otherwise be difficult. Enhanced utensils make eating and cooking easier and self-adjusting mug handles can make drinking easier. However, the issue with these

devices is that they are limited to the specific task they were designed for. Currently, there are few products on the market that eliminate or reduce tremors from the hand itself. The only one currently available is the ReadiSteadi, which uses a system of weights to reduce tremors. There are several systems in development, such as the Steadywear, which uses earthquake dampening technology to eliminate tremors, and the Emma watch, which counteracts tremors with a vibration counter frequency to break the feedback loop in the brain causing tremors. Another product in development is the Gyroglove, which uses a gyroscope mounted on top of the hand to resist the rapid movements of tremors.

The goal of this project is to incorporate the principles of gyroscopic stability to create a device that actively reduces the tremors experienced by the hand. Rotating objects naturally resist motions that attempt to move them out their plane of rotation. The larger the impulse, the larger the resistance force that the rotating object exerts. This means that while it will resist the high frequency movements of tremors, it will allow the motion of steady, deliberate movement. This will allow individuals to experience life without the disablement of hand tremors, and can be universally applied to multiple tasks, rather than one specific function.

2.0 BACKGROUND

This chapter presents background information on hand tremors and current treatment methods. First is an examination of different hand tremor conditions and biological factors that go into a diagnosis. Discussed next are modern treatments for various tremors types. After, products and orthotics are introduced to provide insight on solutions to relieve tremor symptom. Finally, the physics behind the use of gyroscopes to reduce tremors.

2.1 TREMOR CLASSIFICATION: RESTING VS. ACTION

There are two primary classifications of tremor: resting tremor and action tremor. The American Academy of Family Physicians defines resting tremor as occurring "... in a body part that is relaxed and completely supported against gravity" (Crawford, 2011). Resting tremor is diagnosed when the appendage in question is not intentionally stimulated by the individual, yet the body part continues to tremor regardless. Resting tremor can be typically enhanced by things like mental stress, or movement of other body parts, while deliberate actions can cause resting tremor to temporarily subside. Resting tremor is also often referred to as "pill rolling" tremor. This is due to the movement of the hands and fingers resembling the circular movements of rolling small objects, such as pills, in the hands. Resting tremor is most often diagnosed in individuals with Parkinson's Disease (NINDS, 2017).

Action tremor is therefore defined as occurring during voluntary or deliberate movement by the individual of a muscle or appendage. Most tremors types are considered to be classified as action tremors and can be further separated into the following tremor subcategories, some of which overlap.

- **Postural tremor** occurs when the individual is attempting to maintain a specific position against the force gravity, such as holding the arms in an outstretched position.

- **Kinetic tremor** is connected with any deliberate movement, such as opening and closing hands.

- **Intention tremor** is generated with purposeful movement towards and intended target, such as touching the nose with a finger. In most situations, the tremor will get more pronounced as the individual gets closer to their target.

- **Task-specific tremor** is generally reserved for when the individual is performing a skilled, goal-oriented task, such as handwriting or drawing shapes.

- **Isometric tremor** occurs during a voluntary muscle contraction, which is not accompanied by other movement, such as holding a weight in a still position. (NINDS, 2017)

2.2 CATEGORIES OF TREMOR TYPES

Tremors are often categorized by their appearance and where they originate from within the body. When a physician diagnoses a patient, they take into consideration a number of different observations to determine the nature of the tremor. The key elements include whether the tremor is active when the muscle is at rest or contracted, the location of the tremor, and if it is mirrored on both sides of the body. Certain tremor characteristics, such as frequency and amplitude, are also taken into account when diagnosing a tremor. There are over twenty different types of tremors that have been identified; the most common of which are included in this section. It is important to note that many tremor manifestations may be similar, but they are categorized by their root cause.

2.2.1 CEREBELLAR TREMOR

Cerebellar tremor can appear as many other forms of tremor, and manifests itself as a high amplitude, low frequency tremor. This means that it is easily visible and noticeable. Cerebellar tremor causes agitation at the end of extremities, typically at the end of an intentional movement, such as reaching for an object (NINDS, 2017). Cerebellar tremor is a tremor that is caused by damage to the cerebellum and its pathways to other regions of the brain. This damage can be caused by things like heart attacks or stroke. The cerebellum is located at the base of the skull where the brain meets the spinal cord and contributes to the coordination and precision of muscle movements. It is not responsible for initiating movements (Britannica).

2.2.2 DYSTONIC TREMOR

Dystonic tremor is a symptom of the movement disorder *dystonia*. Dystonic tremor occurs due to incorrect message transfer from the brain to the corresponding muscle, causing them to be overactive. Dystonic tremor occurs where the dystonia is located. For example, dystonia in the head or neck and cause the head and neck to rotate or bob back and forth. Dystonic tremor can cause in an individual having abnormal posture or sustained and unwanted movements. It is also more common for dystonic tremor to affect the head and neck, along with other areas, compared to other movement disorders (Elble, 2012).

2.2.3 ESSENTIAL TREMOR

Essential tremor is one the most common movement disorders. Essential tremor primarily affects the hands, and can expand to the head, which can cause stuttering of the voice. Both sides

of the body are typically affected equally, though it can be more pronounced on the individual's dominant side due to essential tremor being an action tremor. For many affected people, the tremor remains mild and constant for many years (NINDS, 2017). The shaking frequency will often decay with age, but the severity or magnitude of the tremor may increase. Individuals affected by essential tremor will often start noticing symptoms during adolescence (10-19), or as middle-aged adults (35-50). At this time, it is unknown what causes essential tremor. Things like heightened stress, fever, and exhaustion can increase its severity, while meditation and small amounts of alcohol can help decrease its severity. There is a fair amount of evidence to support a genetic link, but researchers are currently unsure as to what the specific connection is at this time (Burke, 2018).

2.2.4 ORTHOSTATIC TREMOR

Orthostatic tremor is a rare disorder of erratic and rapid contractions of the legs that tend to occur when the individual is standing. These irregular movements tend to make the individual feel imbalance and unsteady when standing still. When the individual is in a seated position or walking, the tremor will often disappear partially or completely, depending on the severity. Orthostatic tremor is also sometimes referred to as "shaky legs". At this time, it is unknown where orthostatic tremor originates within the body. Current theories presented indicated that it is an offset of essential tremor, genetic causes, or developmental issues experienced by the individual. However, at this time it is unclear as to where orthostatic tremor is caused, and more research is being conducted to understand its origins (Jankovic, 2017).

2.2.5 PARKINSONIAN TREMOR

Unlike most other tremors, parkinsonian tremor is a resting tremor, that can affect any part of the body, including the fingers, hands, jaw, and feet. As defined above, resting tremors primarily affect an individual's appendages when they are at rest. However, Parkinsonian tremor is also very apparent in isometric and task specific situations as well. This makes common tasks like eating soup with a spoon particularly difficult because parkinsonian tremor inhibits the body's ability to make the smooth and precise motions necessary to keep the spoon steady and level. Parkinsonian tremor is also an asymmetric condition, meaning that both sides of the body are independent of the other's condition. Although once one side is affected, it will always remain the more affected side (APDA).

Parkinsonian tremor is a very common side effect of the well-known Parkinson's disease. Parkinson's disease is a degenerative nervous system disorder that affects the movements of the body. Parkinson's is most commonly caused by failed nerve cells within the brain, various genetic mutations that can increase the risk of Parkinson's, or to environmental contaminants, such as exposure to damaging toxins, that can trigger its presence. Along with tremors, Parkinson's disease can also cause slowed movement, rigid posture, impaired balance, and speech impediments (Mayo, 2018).

2.2.6 PHYSIOLOGIC TREMOR

Physiologic tremor is not considered to a be a disease, but merely a normal experience. Physiologic tremor is usually for fine tremors that includes partial shaking of an appendage that experiences rhythmic activities. Things like cutting hair and pressing a sewing pedal over time can create a slight repetitive tremor based on those actions (NINDS, 2017). In these examples,

cutting hair could lead to a slight tremor of restless fingers, and depressing sewing machine pedal may lead to a restless leg when sitting down.

2.2.7 PSYCHOGENIC TREMOR

Psychogenic tremor is not considered to be a disease, but more a side effect of other life conditions or mental disorders, such as stress, post-traumatic stress disorder (PTSD) or depression (NINDS, 2017). Psychogenic tremor manifests as very fine and shaking of any parts of the body. It can appear and disappear abruptly and is much more "responsive" to external input. For instance, it will often disappear when the individual becomes distracted or focused on something else (Crawford, 2011).

2.3 CURRENT TREATMENTS

The nature of tremors has been studied for a long time. In that time, a broad range of treatments have been developed. These treatment styles can be broken down into three main categories: medication, focused ultrasound/radio waves, and surgery. Each have several options that are designed to counteract the effects of specific conditions and have their own advantages and disadvantages. For instance, medications can be very effective at reducing tremors, but often come with unwanted side effects, and can run the risk of individuals developing an immunity to them over time. Magnetic Resonance Guided Focused Ultrasound (MRGFUS) is a rapidly developing field that has recently been implemented to treat a wide variety of tremor disorders. Another effective new surgery is deep brain stimulation, or DBS, in which electrodes are

implanted inside the brain. This section will explain in greater detail the different treatment

options that are available to people with tremor disorders.

2.3.1 MEDICATIONS

Medication is often the first option doctors will prescribe. There are an abundance of

medications for each disorder, and the one selected depends on a variety of factors, such as:

effectiveness, tolerance, health risks and tremor type. Below are details about the various

medications for individuals with two of the most common tremor causing conditions: Essential

Tremor and Parkinson's Disease.

2.3.1.1 ESSENTIAL TREMOR MEDICATIONS

Essential Tremor (ET) is the most common tremor-causing disorder, however there are

currently no specific prescription drugs for the treatment of essential tremor (IETF, 2018).

Medications are instead used are for dealing with ET symptoms. These are pre-existing

medications developed for other conditions, including seizures and convulsions. While these

medications can be effective, they share several large issues that prevent them from being

definitive solutions. The primary problems are that there is a significant lack of understanding of

how these drugs reduce tremors, and as mentioned above, patients can become resistant to the

treatments overtime. The medications are only temporary solutions to symptoms that can be

long-lasting. As of today, the two most prescribed medications fall into two forms: beta blockers

and anti-seizure medications (WebMD, 2018).

Beta blockers are generally used as the first option of medication for essential tremor. It

is speculated that beta blockers, such as propranolol (Inderal), atenolol, metoprolol, and sotalol,

block nerve impulses that cause the tremors (WebMD, 2018). Although the result of taking the medication can be an improvement, this line of medication is effective in 50-60% of patients (Neurology Reviews, 2015). Inderal is the other commonly used beta blockers, and is effective in reducing overall tremors, though does not completely eliminate them. Studies have shown that around 10% of patients who take Inderal for tremors stop benefiting from it after a year of treatment. It is currently unknown why this occurs because it is still not fully understood how it works to treat tremor yet (WebMD, 2018). People taking Inderal have also been found to be unable to tolerate it. This is typical when the other forms of the beta blockers are used. Although in some cases, patients do not respond to these new medications, and/or cannot tolerate their effects either. Inderal and other beta blockers are taken once or twice a day and have relatively minor potential side effects. These typically include drops in blood pressure, fatigue, and erectile dysfunction. If these side-effects occur, they may also require an anti-seizure medication.

If beta blockers are rendered to be ineffective, the next level of medication for essential tremor is primidone, or mysoline. Primidone is an anticonvulsant drug that is prescribed off-label to treat patients with ET. Primidone is effective in approximately 60% of patients, and in some cases can be more effective than beta-blockers. In multiple placebo-controlled trials, primidone was proven to reduce the amplitude of upper limb tremors by 60-66%. However, the reduction of tremors in other areas of the body were not as consistent or conclusive (Lyons, 2015). Primidone is most effective at reducing hand tremors, though in some cases it created worse tremors for certain individuals. It also bears the potential undesired side effects of dizziness, nausea, and fatigue. Primidone also has the potential, although rare, to create a complication with blood cells and bone marrow. It also runs a similar risk to beta-blockers of patients developing an immunity to it after a year or so of treatment (WebMD, 2018).

2.3.1.2 PARKINSONIAN TREMOR MEDICATIONS

Unlike Essential Tremor, Parkinson's Disease does have several medications that are made to directly treat the underlying disease. One of the most popular prescriptions is Levodopa, which has been in use for over 40 years. Levodopa works by entering the brain and turning into dopamine. Parkinson's Disease creates a deficiency of dopamine in the brain, and this lack of dopamine is what causes the tremors to occur. By feeding Levodopa as a supplemental source of dopamine, the tremors are then reduced. It is considered to be largely effective, especially when dopa-decarboxylase inhibitors (DDCI) are taken in conjunction with it.

DDCI drugs, such as Cardidopa, slow Levodopa's peripheral conversion to dopamine, which reduces side effects and increases its half-life, allowing it to be more effective for longer periods of time (Salat, 2013). The treatment is considered to be one of the most effective forms of treatment, however it is not without side effects. These include: somnolence (intense drowsiness), mood changes, nausea, hypotension, vomiting, and in rare cases worsening in their condition and depression (Salat, 2013). Long term Levodopa treatment has been shown to potentially lead to motor complications and dyskinesia. Despite these side effects, its effectiveness in reducing symptoms makes it a preferable option. This may especially appeal to young patients as they typically want to remain employable and physically active for as long as possible (Salat, 2013).
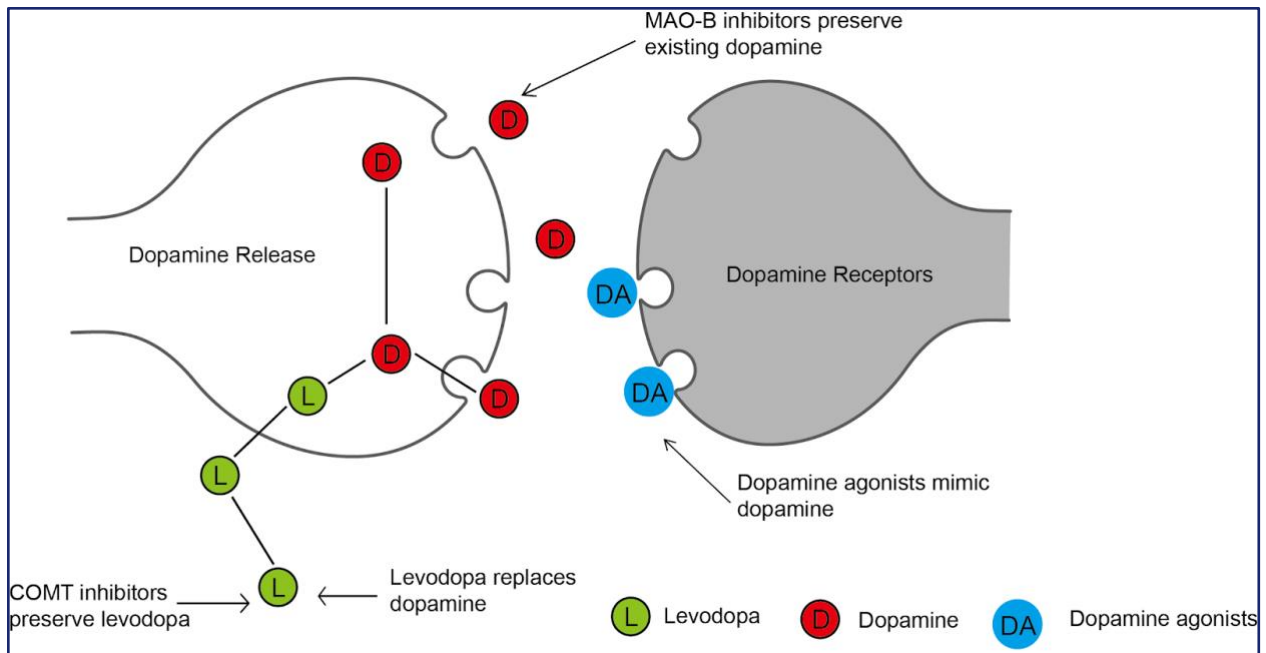
FIGURE 1: MECHANISMS OF PARKINSON'S MEDICATION IN THE BODY (BURBLLA, 2017)

Another common medication is dopamine agonists. This medication works by acting similarly to dopamine in the brain (WebMD, 2018). This line of medication is often tried before Levodopa, as it has a lower risk of causing the development of motor complications. However, after 2 years, around 50% of patients that began treatment using dopamine agonists needed to take Levodopa to supplement their treatment to achieve the same level of symptom reduction they previously experienced with dopamine agonists (Salat, 2013).

It has also been shown in long-term follow ups that initiating treatment with dopamine agonists does not lower patients' risk of developing severe motor complications (Salat, 2013). This treatment is often considered the first option for individuals who develop Parkinson's, especially those with early onset Parkinson's. Individuals with early onset Parkinson's are much more likely to develop motor complications later in life, and so dopamine agonists, which are considered to lower the chances of developing these complications than Levodopa, are generally the first recommendation by a physician. However, this treatment comes with certain behavioral

side effects. These can include impulse control disorder and postural hypotension, which can make it hard to remain active and employable (Salat, 2013).

2.3.1.3 BOTULINUM TOXIN

For a more general form of tremor reduction, injections of Botulinum Toxin, also known as "Botox", have been proven to reduce tremors for up to 3 months at a time (Niemann, 2018). It is naturally produced by the bacteria Clostridium botulinum. Botulinum Toxin causes flaccid paralysis in muscles by preventing the release of acetylcholine, which is the chemical released by motor neurons to signal muscle movement (Arnon, 2001). Use of this toxin has significantly reduced the tremors in muscles suffering due to a fault in these signals. Patients receiving this treatment have been reported to have noticeable improvement in their tremors with limited side effects. This is due to the fact that the treatment is not a general body medication, but a targeted muscle treatment. However, the downside of this treatment is that the targeted and surrounding muscles are left feeling weak. In the case of head and neck treatments, this can cause the individual's voice to become hoarse, and difficulty swallowing.

2.3.2 SURGERY

For tremor causing conditions, there are two main surgical procedures. They are different in their objectives, and the conditions for which one is selected over the other. The first method, thalamotomy, removes part of the thalamus that is causing tremors. It executes the same function as radiofrequency ablation but comes with more risks and is considered less effective, so it is not used as frequently anymore. The second method is deep brain stimulation (DBS). This method

implants electrodes in the patient's brain that send signals to correct the signals causing tremors. This is becoming more popular as testing shows its high level of effectiveness.

2.3.2.1 THALAMOTOMY

Thalamotomy is a procedure that is being used less and less, as it is an inherently invasive procedure which can be done with new developing technologies previously mentioned, such as radiofrequency ablation and MRgFUS. During this procedure a probe is inserted into the patient's brain, and it is used to destroy targeted tissue in the thalamus that is causing tremors to occur. This is done by either circulating liquid nitrogen in the probe or using an electrode to heat it up and denature the defective cells. Thalamotomy can be effective at removing tremors, however it does not help with any other symptoms from the underlying condition (Healthwise, 2017). It also comes with certain risks, such as stroke, numbness around mouth causing drooling, seizures, impaired speech, and cognitive impairment. These serious side effects and the nature of the procedure only fixing tremors and no other symptoms that other developed treatments can address, are large factors into why thalamotomy is not seen in practice as frequently in modern treatment.

2.3.2.2 DEEP BRAIN STIMULATION

Deep brain stimulation, or DBS, is a developing treatment that uses implanted electrodes to eliminate tremors from jumbled signals within the brain. The electrodes are connected to a main hub that is implanted in the chest of the patient, similar to a pacemaker (Mayo, 2018).
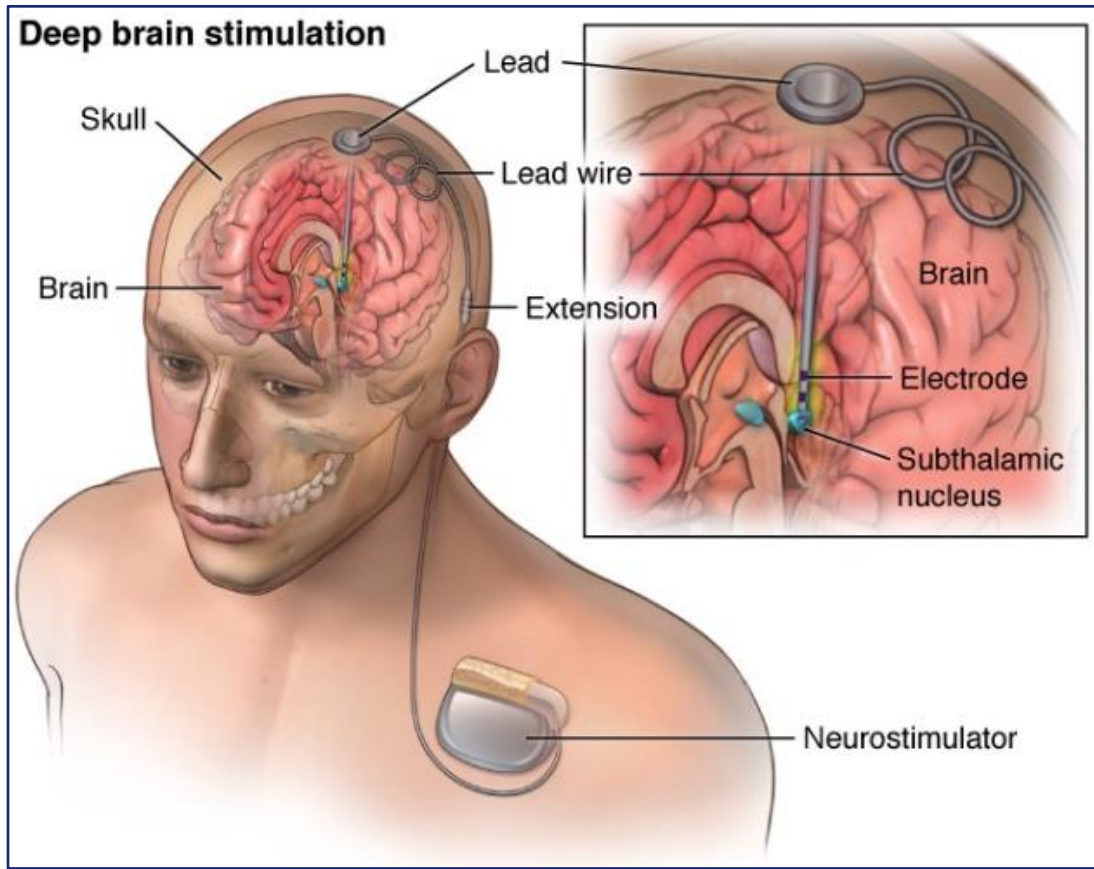
Studies have shown that DBS can be more effective than standard medications. In a study done in 2006, in 50 of 78 pairs, the patient that received were recorded to have their symptoms improved greater than with the patient that received medication (Deuschl, 2006). DBS, combined with its lower rate of occurring adverse effects, (64% frequency in medication group, 50% in DBS group), makes it a promising option for people suffering from Parkinson's and other tremor causing conditions (Deuschl, 2006). The main issue with this treatment is that when adverse events do occur, they can be more serious. Side effects/adverse events can include seizure, infection, and stroke. During stimulation, other side effects can occur as well, such as numbness, tingling, muscle tightness, speech and balance problems, and mood changes (Mayo, 2018). The

treatment is continuously being developed and with improvements to reduce these effects, deep brain stimulation can be a viable option for patients with tremors.

2.3.3 FOCUSED WAVE TREATMENTS

Focused wave treatments are a developing form of treatment that is sought after as an alternative to surgery. Both forms, Focus Ultrasound (magnetic resonance guided focused ultrasound or MRgFUS), and Radiofrequency Ablation, use a treatment method called ablation (Jung, 2018). Ablation is when diseased or malfunctioning tissue is purposely destroyed in order to alleviate a condition. For example, purposely destroying faulty tissue in the heart causing irregular electrical signals to restore proper signal transfer (Joseph, 2012). Both have seen many positive results and are being researched and developed further to bring them more into the mainstream of treatment.

2.3.3.1 FOCUSED ULTRASOUND

Focused ultrasound uses ultrasonic waves to destroy tissue in the ventral intermediate (Vim), nucleus thalamus, and posterior subthalamic regions of the brain. These are the most common areas of the brain that when dysfunctional, typically result in the manifestation of a tremor (Jung, Na Young, 2018). The ultrasonic waves resonate the targeted parts of the thalamus, causing heat energy to build and degenerate of proteins, cause blood to coagulate, and cell necrosis (Jung, Na Young, 2018). Focused ultrasound also causes cavitation. Cavitation is the formation and oscillation of microbubbles within the blood and cell cytoplasm. This in turn damages and destroys the malfunctioning cells in the targeted area (Jung, Na Young, 2018).

Based on a study 2016, the results of the treatments have been largely successful. Tremor scores across clinic decreased from a point average of 18.1 to 9.6 within three months after the procedure. These scores also remained level after follow-up appointments held 12 months after the surgery (Jeffery, 2016). This was said to come with an "acceptable" amount of side effects, which included dizziness, nausea/vomiting, ataxia, and paresthesia. Despite these potential side effects, most patients reported a favorable reduction in tremors and a "much improved daily life and quality of living" (Jeffery, 2016).

2.3.3.2 RADIOFREQUENCY ABLATION

Radiofrequency ablation is similar to focused ultrasound in that it uses resonating frequencies to destroy targeted tissue. This method is an adapted version of a surgery called a thalamotomy. During the procedure, a radio frequency is sent into the brain to create an electrical current to heat up a nerve inside the thalamus. This disrupts its ability to function for at least 6 months and alleviates the symptoms of certain conditions such as essential tremor and Parkinson's (Elble, 2018).

2.4 PRODUCTS FOR HAND TREMORS

This section presents a selection of products that are on the market, or currently in development. Assistive products are categorized into two main categories: passive and active. A passive device resists a tremor without moving parts. These designs utilize intentional design features to aid the individual with a specific task. Active devices counteract tremors in real time. They utilize sensory or motion input from the body to generate a counteractive response to the

tremor. From here, products can be further separated into tools and wearables. Tools are defined as products that are intended for the individual to use to carry out a particular function. A wearable refers to a product that an individual mounts or straps to their body to reduce tremors. Wearables may also be referred to as an orthosis or orthotic, which is defined as an externally applied device used to modify the structural and functional characteristics of the neuromuscular and skeletal system.

2.4.1 PASSIVE ASSISTIVE DEVICES

Passive devices for hand tremors are usually an ergonomic improvement or a weighted object designed to aid the movement of the user. One of the most challenging tasks for individuals with hand tremors is dexterity, which is required for conducting simple, everyday tasks like using utensils. The S'up Spoon, seen below in Figure 3, is a product that took the functional purpose of a spoon, and redesigned it to accommodate for individuals unable to hold their spoons steady. The first feature is the thicker, smooth handle which increases contact area with the hand. The second feature is the hollowed cavity for the scoop part of the spoon. This allows users bring food to their mouths without spilling (S'up, 2018).

Another feature is increasing the mass. The idea is that through conservation of momentum, increasing the mass of a system will decrease the velocity. In this case, solutions like those of Keatlery Weighted Utensils, have altered the weight of their utensils to about 8 ounces. The added weight slows hand movements, thus dampening the effects of the individual's tremors when eating (Keatlery Weighted Dining Utensil, 2018).

Similarly, with the S'up Spoon, the Rocker Knife, seen below in Figure 4, utilizes different geometries to aid an individual's ability to cut food. It uses an arced blade that is rocked back and forth. A T-shaped handle is attached to the backside of the arc, placing the user's hand above and away from the cutting surface. This design is much easier for an individual with hand tremors to grip, as well as use to cut food items (Rocker, 2018).

Other eating solutions include the Eatwell Assistive Tableware Set and the Stay Bowl. The two products utilize slip-resistant and anti-tip features to improve their stability. The tableware set has weighted and slanted bottoms with deep cavities to naturally congregate food. Their spoons are designed to match the contour of the bowls to ease scooping (Eatwell, 2018).

Another approach, called the SteadyRest, uses a plastic bracket secured to the wrist, and extended to the palm of the hand. When holding a utensil, the item is supported by the bracket at a notch at one end. This essentially moves the support away from joints in the fingers and the wrist to the forearm, bypassing the tremors in the hand. In the closed-grip position, seen to the left side of Figure 5, the bracket extension adds rigidity to the hand. In the free grip position, seen right of Figure 5, the bracket adds a support point towards the end of the utensil, causing any hand tremors to minorly move the end of the utensil, rather than shake uncontrollably (SteadyRest, 2016).

Similar to how weighted utensils dampen tremor, the Readi-Steadi is a wearable orthotic that straps weights to the hand, wrist, and up to the elbow if desired. The Readi-Steadi system uses custom weights to reduce undesired tremor movements. Meant to reduce mild to severe tremors, the weights effectively reduce the magnitude of the tremor by slowing down the arm (Readi-Steadi, 2016).

2.4.2 ACTIVE ASSISTIVE DEVICES

Active products resist or reduce tremors by producing a counter movement or force. Products in this category contain moving parts and/or electronics that control the device's reaction to a tremor.

Liftware Steady is a smart modular utensil with a variety of utensil attachments for eating. The device, seen below in Figure 6, uses active stabilization on the utensil end using advanced sensor and motor-based cancellation technology. Sensors within the handle measure the magnitude and direction of the motion generated and adjust the utensil end appropriately to keep it as level as possible. The highly sophisticated system is able to reduce tremors to the utensil by

70%. The Liftware Level is a second product by Liftware that stabilizes hand and arm tremors with a more versatile joint to connect the utensil end to the handle (Liftware Steady, 2018).

FIGURE 6: LIFTWARE STEADY (LIFTWARE, 2018)

The Steadiwear glove, shown below in Figure 7, aims to universally reduce hand tremors in the wrist and forearm using a ball joint damper. This technology is similar to that used to stabilize buildings and structures against earthquakes. The joint contains a dampening fluid that resists the impulses generated by tremors. The developers say that it reduces movements of a frequency greater than 2 Hz (2 movements per second) and does not provide as much resistance to movements less than 2 Hz. The system allows for full range of motion, while resisting tremors in the directions observed to be most common for Parkinson's disease and Essential tremor (Steadiwear, 2018).
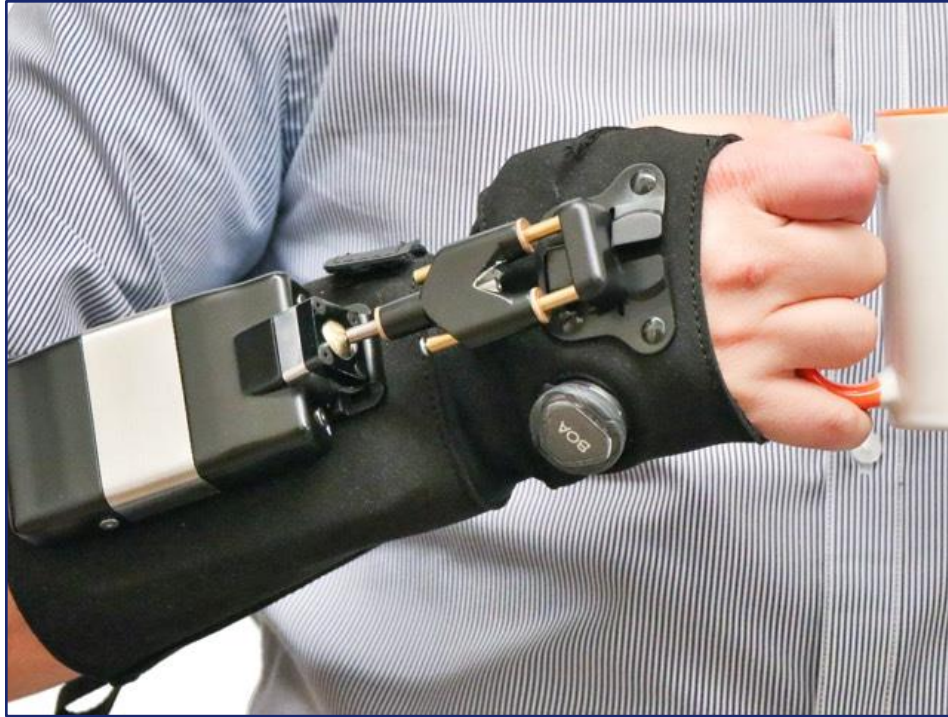
FIGURE 7: STEADIWEAR GLOVE (STEADIWEAR, 2018)

The GyroGlove uses a gyroscope to stabilize the hand via gyroscopic stability from angular momentum. Gyroscopic stability is defined as "the resistance of a rotating body to a change in its plane of rotation" (Kent, 2016). Angular momentum refers to the rotational equivalent of linear momentum, where angular velocity is multiplied to the inertia of the spinning mass. In the GyroGlove, the spinning mass and motor are mounted to the back of the hand in an enclosed assembly. As the hand experiences a tremor, the stability of the gyroscope helps to resist tremor movements by keeping the gyroscope spinning in the same plane. The mass is designed so that small tremor movements are resisted by the gyroscopic forces yet allows for intentional and deliberate movements to occur (Simon, 2016).

2.5 PHYSICS OF A GYROSCOPE

Gyroscopic stabilization works by responding to an input torque with an equal and opposite reaction torque. When a torque acts on a gyroscope and attempts to move it off of its spin axis, the spinning of the gyroscope generates another torque that acts orthogonally to this input torque. This motion is known as precession. Precession generates an additional torque that resists the original input torque. It is the generation of this resistance torque that is opposite and proportional to the input torque that is the basis of the final design.

To understand the capabilities of the design, it is important to review the physics of the system. One of the fundamental properties of how gyroscopes operate is angular momentum. That is the product of an object's moment of inertia and angular velocity. This is displayed in Equation 1 below.

$$\bar{L} = I_g * \bar{\omega}$$

This equation follows Newton's First Law; a gyroscope maintains its angular momentum unless an external force acts upon it. This means that a gyroscope will naturally maintain its angular velocity and by extension, its plane of rotation. In order to change the angular velocity of the gyroscope, an external moment must be applied, as seen in Equation 2.

$$\Sigma \overline{M_g} = \frac{d(I_g * \bar{\omega})}{dt}$$

The moment of inertia (I) is the tendency for a rotating object to maintain its angular velocity based on its geometric properties. The equation for moment of inertia is shown below as Equation 3, in which c is the geometric coefficient:

$$I = c * m * r^2$$

By determining the moments of inertia, the acting torques in the system can be calculated. This is because torque is equal to the change in angular momentum with respect to

24

time. This relationship can be seen below as Equation 4, which is derived by simplifying

Equation 2 by replacing the moment variable (m_g) with torque (τ) and converting the moment of

inertia and angular velocity to the change in angular momentum.

$$\bar{\tau} = \frac{\Delta(c * m_g * r^2 * a)}{\Delta t}$$

To determine the direction and magnitude of the output torque in the gyroscopic system,

the team adapted a model developed by Brendon Allen at Brigham Young University. Allen

conducted analyses on different gyroscope configurations to determine a theoretical optimal

design of a gyroscopic tremor suppression device. The basis of his model is shown in Equation 5,

(Allen, 2018).

$$H * q_{acc} + C = F$$

In this equation, H represents the moments of inertia of the gyroscope about different

axes. The q_{acc} signifies the angular acceleration of the hand caused by the tremor and the

gyroscope due to the subsequent precession. Multiplied together, $H*q_{acc}$ equals the torques

caused by the motion of the hand. C represents the torques created by the movement of the

system. The resultant torques about the axis of rotation and precession axis are represented by F.

The expanded version of the H and C components are shown here:

$$H := \begin{pmatrix} m_f \cdot x_p^2 + m_f \cdot y_p^2 + m_f \cdot r_f^2 \cdot \cos(\phi)^2 + 2 \cdot m_f \cdot y_p \cdot r_f \cdot \cos(\phi) + I_{xf} \cdot \cos(\phi)^2 \ldots & -m_f \cdot x_p \cdot r_f \cdot \sin(\phi) \\ + I_{yf} \cdot \sin(\phi)^2 + m_w \cdot x_w^2 + I_{zw} + m_f \cdot x_p \cdot r_f \cdot \sin(\phi) & \\ -m_f \cdot x_p \cdot r_f \cdot \sin(\phi) & m_f \cdot r_f^2 + I_{zf} \end{pmatrix}$$

$$C := \begin{pmatrix} -2 \cdot m_f \cdot \omega \cdot \varphi \cdot r_f^2 \cdot \cos(\phi) \cdot \sin(\phi) - 2 \cdot m_f \cdot y_p \cdot r_f \cdot \omega \cdot \varphi \cdot \sin(\phi) - 2 \cdot I_{xf} \cdot \omega \cdot \varphi \cdot \cos(\phi) \cdot \sin(\phi) \ldots \\ + I_{yf} \cdot \Omega \cdot \varphi \cdot \cos(\phi) + m_f \cdot g \cdot x_p \cdot \cos(\theta) - m_f \cdot G \cdot y_p \cdot \sin(\theta) + m_w \cdot G \cdot x_w \cdot \cos(\theta) \ldots \\ + -m_f \cdot G \cdot r_f \cdot \cos(\phi) \cdot \sin(\phi) - m_f \cdot x_p \cdot r_f \cdot \varphi^2 \cdot \cos(\phi) + 2 \cdot I_{yf} \cdot \omega \cdot \varphi \cdot \sin(\phi) \cdot \cos(\phi) \\ m_f \cdot \omega^2 \cdot r_f^2 \cdot \cos(\phi) \cdot \sin(\phi) - I_{yf} \cdot \omega^2 \cdot \sin(\phi) \cdot \cos(\phi) + I_{xf} \cdot \omega^2 \cdot \cos(\phi) \cdot \sin(\phi) \ldots \\ + m_f \cdot y_p \cdot r_f \cdot \omega^2 \cdot \sin(\phi) - I_{yf} \cdot \Omega \cdot \omega \cdot \cos(\phi) - m_f \cdot G \cdot r_f \cdot \sin(\phi) \end{pmatrix}$$

The variables were determined based on a combination of research, hand calculations, and Solidworks analysis based on the final design. A study by Calzetti et al. measured these values for Essential Tremor, one of the most common forms of tremor that act about a central oscillator, in the form of displacement from the vertical plane. The average and extreme angular displacement of the hand is 3.2 and 32 degrees respectfully. The frequency range is from 3-6 hertz (Calzetti, 1987). This value was then used to determine the angular velocity of the hand. Angular displacement of the tremor is divided by its corresponding frequency, shown in Equation 6.

$$\omega = \frac{\theta}{f}$$

For the angular acceleration of the hand, rather than finding the average acceleration by using the change in velocity over time, the team solved for the hand's instantaneous acceleration. This is more accurate to the motions occurring in a real tremor given the nature of a tremor to cause sudden small movements. Rearranging Equation 1 solves for the acceleration based on the input torque, Tw.in, shown as Equation 7.

$$q(\theta) = \frac{T_{w.in}}{I_{zs}}$$

A similar reconfiguration of Equation 1 solves the angular velocity of the gyroscope as it is rotated about the precession axis, shown below as Equation 8.

$$\varphi = \frac{T_{w.in}}{I_{yf} * \Omega}$$

3.0 GOAL STATEMENT AND PRODUCT SPECIFICATIONS

The goal of this project was to create an assistive system that uses a gyroscope to stabilize hand tremors for use in multiple applications. Listed below are the design goal specifications set by the team at the start of this project.

- Hand Mount:

    o Weigh under 1 lb. (453.6 grams)

    o Allow for full flexible wrist movement

- Sound:

    o Under 80 decibels from 6 inches away

- Dimensions:

    o Height: Under 50 mm - Aim to keep the height as short as possible.

    o Length: Under 70mm - Contained between the knuckles and the wrist

    o Width: Under 70 mm - Contained between the pinky and forefingers knuckles on the average female's hand,

- Effectiveness:

    o Reduce hand tremor magnitude by 70%

- Sensors

    o Successfully identify "hand tremor" patterns

4.0 PROTOTYPE 1

This chapter describes the design of the team's first prototype. The pages below describe the design ideas behind each aspect of the design, including how it is powered, controlled, assembled, and shaped.

4.1 ELECTRONICS

This section discusses all of the electronic systems and components used to control and power the gyroscope. The different subsystems are broken down into power, control, sensory, and data processing.

4.1.1 POWER SYSTEM

The role of the power system is to supply energy to the motor to spin the gyroscope. The power system is essential in creating the rotation needed to counteract the torque generated by hand tremors. The three components of the power system are: the power supply, the speed controller, and the motor. Each component was carefully selected using a decision matrix to compare competing products, and to ensure compatibility to avoid damaging other components.

The motor is the primary component that underwent an arduous selection process. The team began with selecting the motor before anything else, as it would influence other aspects of the system. Factors such as motor type, size, revolutions per minute per volt (kV) all affect the performance of the motor. The decision was first made to select a brushless motor instead of a brushed motor type. Brushless motors have significant advantages over brushed which include higher efficiency, longer lifespan, and little to no maintenance. They do not have components

that contact each other during rotation, whereas brushed motors use brushes inside the motor that can wear and create friction, and therefore heat. The team went to scout for brushless motors in online hobbyist drone markets. With the rise of the drone industry in the past few years, the abundance and competition of the motors in the drone market provided a wide variety of options. Sixteen motor candidates were considered and were then reduced to the top five strongest candidates. The specifications of these can be found below in Table 1.

TABLE 1: SPECIFICATIONS OF TOP FIVE MOTOR CANDIDATES

Motor Name	kV	Battery (S)	RPM	Dia. (mm)	HGT (mm)	Price ($)
Brother Hobby R3 2207 2400kV	2400	5	44400	24 mm	20	19.99
T-Motor F60 III 2207 2750 kV	2750	5	50875	25	-	24.90
PyroDrone HyperLite 2405-2722	2722	5	50357	-	-	22.99
EMAX Lite Spec LS2207 2550 kV	2550	5	47175	27.5	31.2	22.99
Brother Hobby Avenger 2507	2450	5	45325	28	35	25.99

After careful consideration, the Brother Hobby R3 2207 2400kV brushless motor was selected and can be seen below in Figure 8.

FIGURE 8: HOBBY R3 2207 2400KV BRUSHLESS MOTOR (BROTHERHOBBY, 2018)

This motor has a battery rating of 3-5S, which defines the voltage range the motor can receive from the battery. For this motor, the voltage range is 11.1-21V. The kV rating of 2,400 indicates that combined with the maximum voltage rating, the theoretical maximum RPM is 44,400 RPM. The dimensions of the motor are 24 mm in diameter and 20 mm in height. With the motor selected, the next objective was to select the rest of the components.

The electronic speed controller (ESC) is required for driving and controlling the brushless motor. The ESC receives a pulse width modulation (PWM) signal that controls the ESC's output to the motor, which controls the motor's speed. When selecting the speed controller, two factors were required to ensure compatibility with the motor: maximum continuous current, and input voltage. Continuous current refers to the current draw of the motor. Based on the stall current of the motor, which is the maximum current the motor requires, the team was able to select an acceptable speed controller that could provide the motor with the required current. For an increased safety factor, it is better to choose an ESC that is rated for a higher continuous current

than the stall current of the motor to avoid an ESC failure. The second factor, input voltage, refers to the required power supply voltage. The ESC selected was the YEP 60A (2~6S) SBEC Brushless Speed Controller and can be seen below in Figure 9.

FIGURE 9: YEP 60A (2~6S) SBEC BRUSHLESS SPEED CONTROLLER (YEP, 2018)

To provide power to the system, the team decided to use a rechargeable battery for the benefit of its portability. As mentioned above, the battery specifications are depended on the brushless motor and ESC specifications. The other factors considered were the type of battery and the battery capacity. For the type of battery, the energy density and output current are the driving characteristics for consideration. A lithium polymer (LiPo) battery has the highest energy density compared to other batteries currently available on the market. Based on our system requirements, the Turnigy 5000mAh 5S 30C Lipo battery was selected. The 5S refers to the battery's 5 cells in arranged in series, where each cell has a nominal voltage of 3.7 volts. This battery was also chosen for its large 5000mAh capacity, as higher capacity directly increases the

potential runtime of the motor. The Turnigy 5000mAh 5S 30C Lipo battery can be seen below in Figure 10.

4.1.2 CONTROL SYSTEM

The control system is responsible for controlling the power system's ESC. The initial goal was to make the control system adaptive to hand tremors. This meant that if the system detected severe or high amplitude hand tremors, it would increase the RPM of the motor, and when minimal or less severe tremors were detected, the system would decrease the RPM of the motor.

To control the RPM of the motor, the ESC requires a pulse width modulation (PWM) signal. This is accomplished using a HJ digital servo tester to create a variable PWM signal. The range of the length of the signal pulse was between 800 and 2200 microseconds with a frequency of 50 Hz. A digital monitor shows the signal pulse and is controlled by a potentiometer built in.

4.1.3 SENSOR SYSTEM

To create an adaptive control system, sensors are required to provide input data. As mentioned above, an Arduino microcontroller was used to interface with the sensors. Listed below are the sensors that were selected for this project and their capabilities.

Gyroscopic stability is generated through the angular velocity and moment of inertia of the gyroscope. However, the moment of inertia remains constant, whereas the RPM of the disk can be manipulated. Three main types of tachometers to measure the RPM of a spinning object were found currently available on the market: mechanical, optical, and stroboscopic. The optical tachometer, which uses an infrared (IR) emitter and receiver unit wired to an integrated chip, was selected for the purposes of this project. For the IR sensor to detect speed, a reflective tape or surface is required over a portion of the rotating surface. When the emitter produces an IR signal, the tape reflects the signal to be read by the receiver. Each time a reading is made, one revolution has passed.

Hand tremors are motions that are rotating about the center of the hand. An inertial measurement unit (IMU) was used to effectively measure that motion. An IMU contains a micro-electromechanical system (MEMS) accelerometer and gyroscope transducer to measure translational and rotational motion. There are many factors to consider when selecting a transducer relevant to measuring hand tremors. The primary factors are axis, range, and resolution. The axial parameter refers to the number of directions in which translational and angular acceleration can be measured. Range refers to the upper and lower limits of what each sensor can measure. For the purposes of this project, the average frequency for hand tremors occur at 3Hz or greater (Elble, 2016). Resolution refers to the detail of a measurement when

converting an analog voltage to a digital value. For this project, the six axis MPU 6050 was selected. It has a range of +/16g on the accelerometer and +/- 2000 deg./sec on the gyroscope.

It is also important to mention because the motor speed also depends on the input voltage of the power source, a voltage sensor was connected to the battery. This measures the battery voltage and informs the system on the capacity of the battery in real time

Figure 11 below shows the wiring diagram for the sensor system. The microcontroller is the Arduino in the center left. The voltage sensor is in the top left of the diagram. The RPM sensor is in the top right corner of the diagram. Finally, the MPU 6050 accelerometer and gyroscope is in the right side of the diagram. The voltage is measured by the Arduino in the analog input using the yellow wire. The RPM sensor is powered from the 5-volt rail and connected to ground. The digital signal is connected by the white wire to digital input (DI) 2 which is uses the timer interrupt on the Arduino. The MPU 6050 utilized the 3.3V rail to power the chip and is connected to ground. The purple wire connects SCL on the MPU 6050 to the analog in (AI) port 5 and the orange wire connects SDA to AI port 4. The blue wire connects INT to DI 3. The pink wire is connected to the ESC, which is not shown for PWM control of the motor.
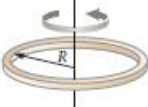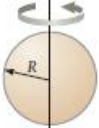
FIGURE 11: SENSOR WIRING DIAGRAM

4.1.4 DATA PROCESSING SYSTEM

The purpose of the data processing system is to log sensor data and provide input to create the adaptive response. Based on the sensory input, analyses can be done to determine the characteristics of the tremor, and the effect of the damping provided by the disk.

In the control and sensor system, the Arduino microcontroller is used to interface and manipulate the gyroscope speed. After comparing microcontrollers and microprocessors, the team found that conjoining the two can provide benefits of both controller and processor. The predominant difference from a microprocessor to a microcontroller is that the former is a computer whereas the latter simply follows code. The premise being that the controller sends sensor data to the computer, the computer can log and transform that data, and decide how to respond if it detects a hand tremor. The microprocessor selected was the Raspberry Pi 3.
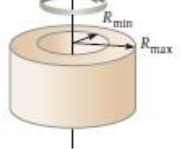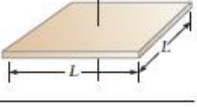
The idea is to filter data from the accelerometer and gyroscope using a Fast Fourier Transform (FFT). Fourier's theorem states that almost any continuous sinusoidal signal can be represented by weighted sum of sines and cosines. Since tremor is an oscillatory motion that is roughly sinusoidal, the tremor can be mathematically decomposed into sine and cosine waves. A plot can then be created featuring amplitude as a function of frequency, creating an amplitude frequency spectrum. In this spectrum, the frequency and amplitude of the tremor can be computed, and the program can automatically draw conclusions from that information.

4.2 DESIGN OF THE GYROSCOPE

Another part of the system to design was the gyroscope itself. This component is very important, because its properties determine many factors of the final design such as weight, comfort, noise, and effectiveness. In order for the device to be effective, the gyroscope had to have a large enough moment of inertia so that it could generate a stabilization force. However, it had to be as small and lightweight as possible as to minimize its bulkiness and weight. Special consideration was needed when the gyroscope was being manufactured as well. Due to the high operating RPMs, small deformities in the gyroscope could cause the gyroscope to oscillate at a high frequency. This could create prominent vibrations that make the device loud, uncomfortable, and less effective.

The design of the gyroscope uses the principles of moments of inertia to maximize its angular momentum while being as small and lightweight as possible. The moment of inertia of an object is determined by its shape and mass, as discussed earlier in Section 2.5. Figure 12 shows the geometric constants, c, for various geometries as they spin on a central axis. In order to maximize the moment of inertia while keeping the weight to a minimum, the team designed

the gyroscope to be as efficient as possible. This was done by combining the shape of a ring, the

geometry with the highest geometric constant, with a disk, which has the second highest constant

of and provided a contact point to the motor shaft.

TABLE 8.2 Moment of Inertia for Some Common Objects

Object	Shape	Object	Shape
Hoop $I = mR^2$		Rod pivoted at center $I = \frac{1}{12}mL^2$	
Solid sphere $I = \frac{2}{5}mR^2$		Pulley/cylinder/disc $I = \frac{1}{2}mR^2$	
Spherical shell $I = \frac{2}{3}mR^2$		Wheel or hollow cylinder $I = \frac{1}{2}m(R_{max}^2 + R_{min}^2)$	
Rod pivoted at one end $I = \frac{1}{3}mL^2$		Solid square plate with axis perpendicular to plate $I = \frac{1}{6}mL^2$	

Note: In each case, *m* is the total mass of the object.

FIGURE 12: MOMENT OF INERTIA FOR COMMON OBJECTS

Figure 13 below shows the top of the gyroscope, showing how the top is a disk to connect

to motor shaft. The following figure, Figure 14, shows the bottom of the gyroscope, and how it is

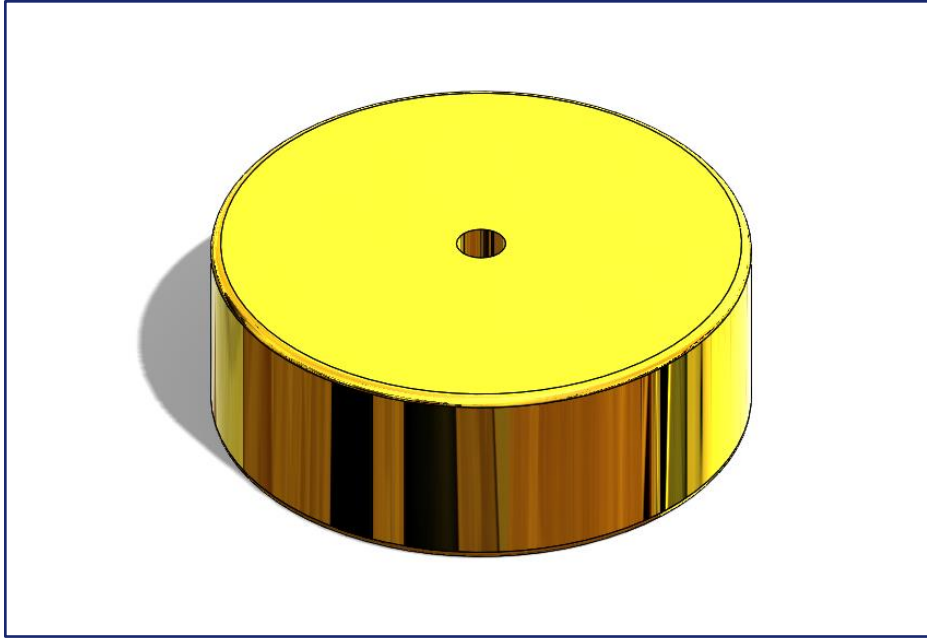designed to be as near the shape of a ring as possible.

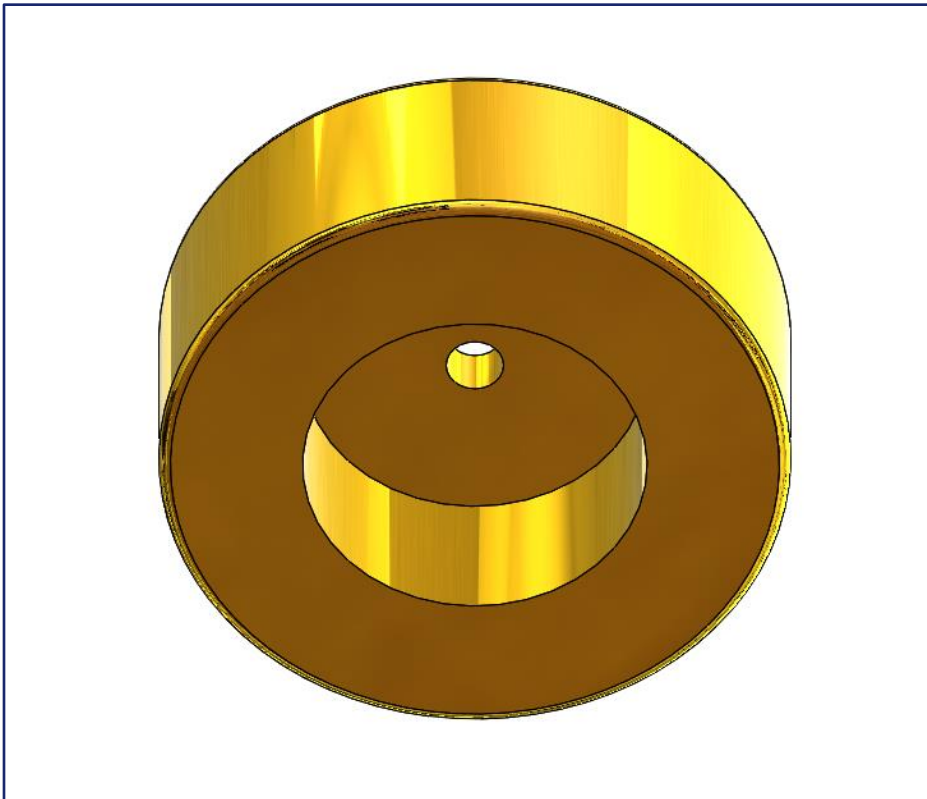*FIGURE 13: GYROSCOPE IN SOLIDWORKS VIEW FROM TOP*

FIGURE 14: GYROSCOPE IN SOLIDWORKS VIEW OF BOTTOM

This was achieved by taking a standard disk shape and cutting a wide shaft on the flat face into the center that almost goes through the disk. Enough mass was left in the center to allow a sturdy connection point between the shaft and the motor, which sits in a center shaft hole. The design of the gyroscope also allows for the motor to sit inside of the mass, conserving space.

The gyroscope was manufactured out of brass, which is the material with the highest density that the WPI Machine Shop was capable of cutting. The team chose to maximize the density of the gyroscope because it would allow for maximum moment inertia while taking up a minimal amount of space. In an initial design phase, the gyroscope was made using a CNC mill, which resulted in the surfaces of the gyroscope being made uneven and left a rough surface finish. When spun at high RPMs, this rough finish caused the gyroscope to generate a high level of vibration and noise. In order to prevent this, the team decided the gyroscope should be manufactured using a CNC lathe. By using a lathe, the gyroscope can be made with a much smoother process that generates even cuts and with a highly fine surface finish.

Another important consideration in the manufacturing process is the fit between the motor axle and the gyroscope. In order to do this, the team decided that a shrink fit would work well to ensure that the gyroscope would fit tightly on the shaft and be as centered as possible. A shrink fit works by creating a hole that is smaller than the shaft that will be inserted into it. The piece is then heated to expand the material until the desired hole is large enough to fit over the shaft. Once inserted, the shaft hole then cools, creating a centered, tight fit. In order to calculate the shrink fit characteristics, the equation for thermal expansion, shown here in Equation 9, was used to calculate the size the hole would have to be at room temperature.

$$D_o = D_{in} * (1 + (T_2 - T_1))$$

After taking measurements with a micrometer we determined the shaft of the motor to be 4.953 mm. A MathCAD file was coded to determine the size the hole needed to be in order to create a proper shrink fit. These calculations can be seen in Appendix A. During the calculations, the team also took into account the various tolerances of the tools that were used to make measurements, as well as of the manufacturing tools themselves. This is highly important considering the size of the dimensions involved. With these calculations, it was determined that the shaft hole needed to be 4.93 mm. In order to achieve such an exact hole size, a custom carbide reaming tool was ordered from Walter Titek. A reamer is a tool that can be used to create an accurate hole size after an undersized initial hole is drilled out. The reamer is capable of creating a hole that is toleranced to +.0004mm of 4.93. Given the various tolerances, a 4.93mm reamer would create a hole that would expand to be + .0012 mm in the best case and -.0008mm, in the worst case, which was determined to be acceptable as that level of interference fits into the "sliding fit" category so the shaft would still fit.

4.3 DESIGN OF THE CASING

The functionality of the casing is to act as a way to house the vital components in an enclosed body, and to secure the mechanism to the individual's hand. The team first began our designing of a casing with a set of functional requirements that the case had to meet. Firstly, the case had to be a rigid structure to house all of the necessary components that would be located on the hand. This included the gyroscope, motor, and various electrical sensors and components. The case had to appropriately fit on top of the hand. The team wanted to make the case large enough to house the necessary components, but to not make it bulky so that it would be cumbersome and unnecessarily large. Based from measurements of the team's own hands, it was

determined that the maximum dimensions for the casing would be 65mm wide, 65mm deep, and 50 mm tall (2.56in x 2.56in x 1.97in). Lastly, the case needed to have an ergonomic fit on the hand. The team wanted to have the case fit as comfortably on the hand as possible and have the ability to match as many of the hand's geometries as possible to make it a normal fit.

To make the inside of the case easily accessible, the casing was made it in two separate parts: the base and the cover. The initial base design can be seen below in Figure 15. The base features a number of design elements that fulfill the design requirements listed above. In the center of the base is a circular cut out with a rectangular channel that leads to the base's edge. This is to create a cavity for the motor to sit in, as well as provide access for the motor's electrical wires to exit the internal cavity. Holes in this central cavity allow for the motor to be screwed into the base to secure its movement. The four hexagonal holes at the corners of the base are for securing the base and cover together. Quarter inch wide nuts were countersunk into them, which corresponds to holes in the cover for screws to hold the two pieces together. The four loops, two on the left and right sides of the base, are used to secure the assembly to the hand. The attachment mechanism used in this first model utilized Velcro straps that wrap around the hand
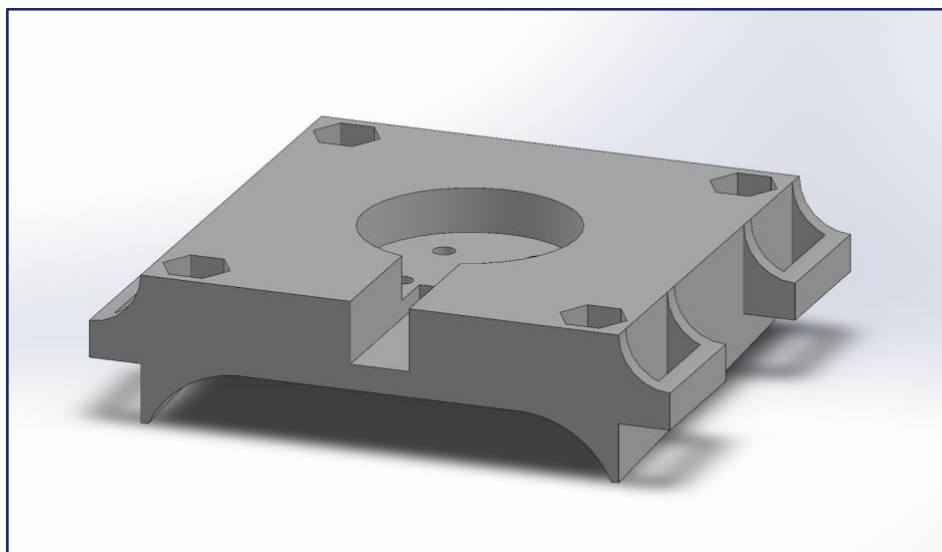

FIGURE 15: INITIAL BASE MODEL

The two flanges, seen below in Figure 16, form the ergonomic geometries that follow the curvature of the hand. The face with the slot where the wires exit the base faces towards the wrist. The flange starts being deeper at this end and gets shallower as it moves towards the opposite face, which is closest to the knuckles. The curves on the flanges adjust across the surface of the hand to adjust with the changes in curvature at the wrist compared to that at the knuckles.
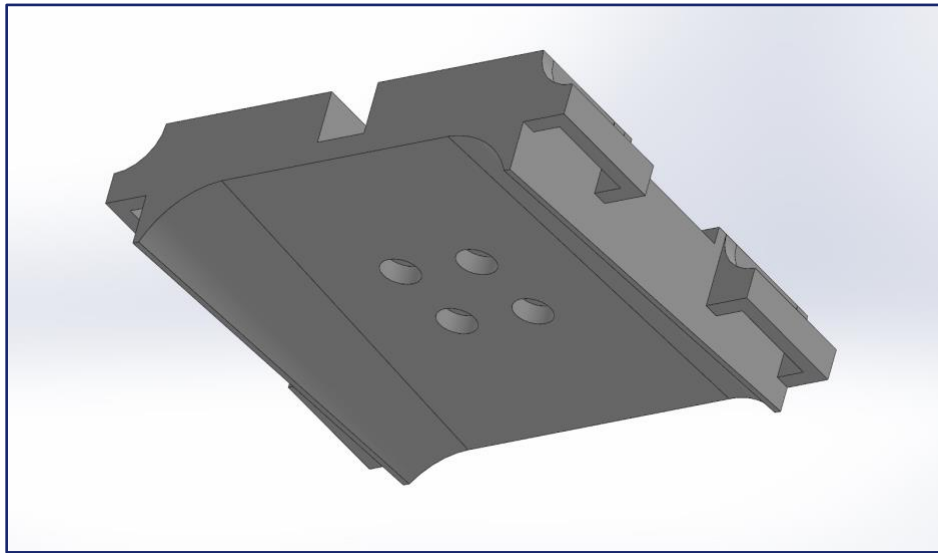

FIGURE 16: BASE MODEL UNDERSIDE

The next addition made to the base model was to add a slot to mount the gyroscopic sensor. The slot is located in the middle of the right side and has to cylindrical bosses that align with mounting holes on the sensor. This change can be seen below in Figure 17.
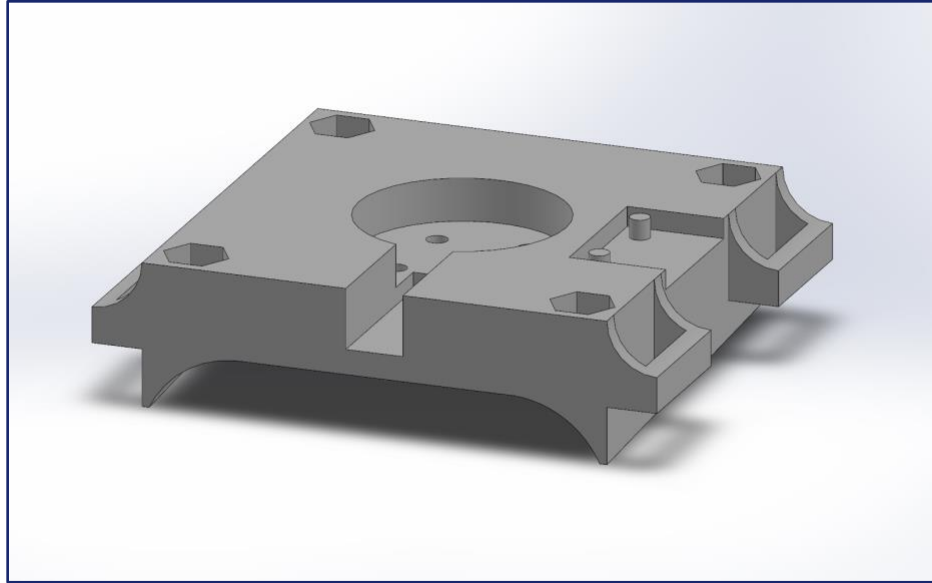
For designing the cover, the initial model was a hollow cylinder to cover the mass and motor, with square flanges that mirrored the base profile. These edges are also where the mounting holes were located, where bolts could pass through and screw into the nuts countersunk into the base. The bottom, walls, and roof of the cover are 8mm, 2mm, and 2.5mm thick respectively. With the outside diameter of the casing being equal to the width of the base at 65mm, these dimensions leave about 3 mm of clearance between the gyroscope and the inner wall of the cover. The vents on the top surface of the cover are too allow for air to circulate and flow in the cavity and help to cool the system. As air was not being actively drawn into the cavity, the team relied on the fast rotation of the motor and gyroscope to add turbulence to the air to increase the rate of cooling. This model can be seen below in Figure 18.
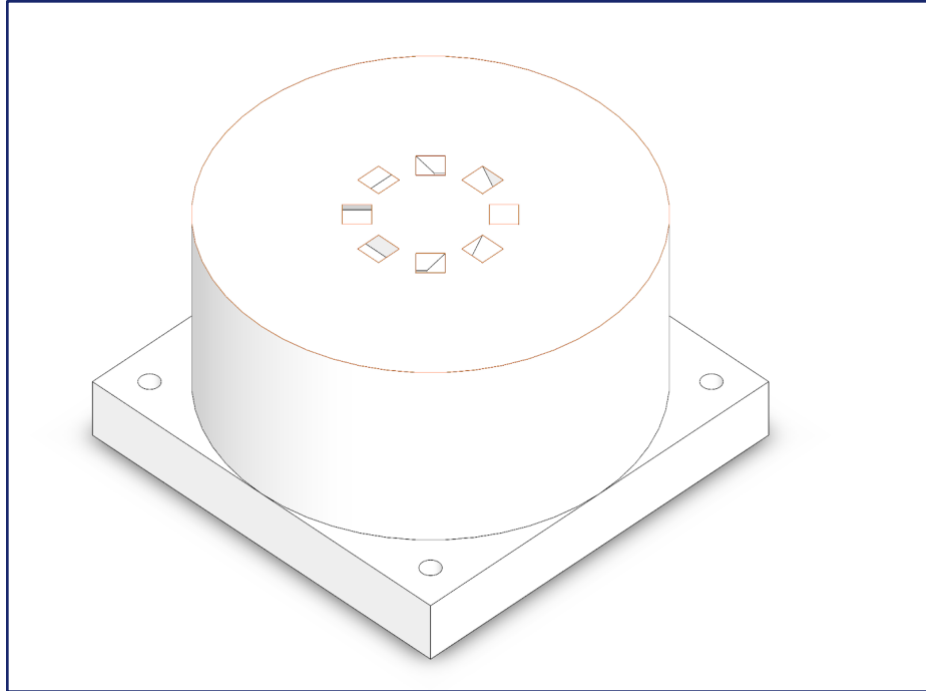
FIGURE 18: INITIAL COVER MODEL

Similar to the base, some adjustments had to be made to the cover to accommodate an infrared RPM sensor. The sensor came mounted on a small 32mm x 14mm electrical chip, with the sensor mounted at one end. When attempting to mount the chip to the cover, there was no good orientation that would securely hold the chip in place without adding a large geometric feature. The solution was to snip the connections from the chip to the infrared emitter and receiver, which was contained within a 5.64mm x 10.14mm x 9.76mm casing. This was a much more manageable size to mount to the motor. As seen below in Figure 19 below, the small sensor end can easily fit onto the side of the cover, without creating any extensive geometries.
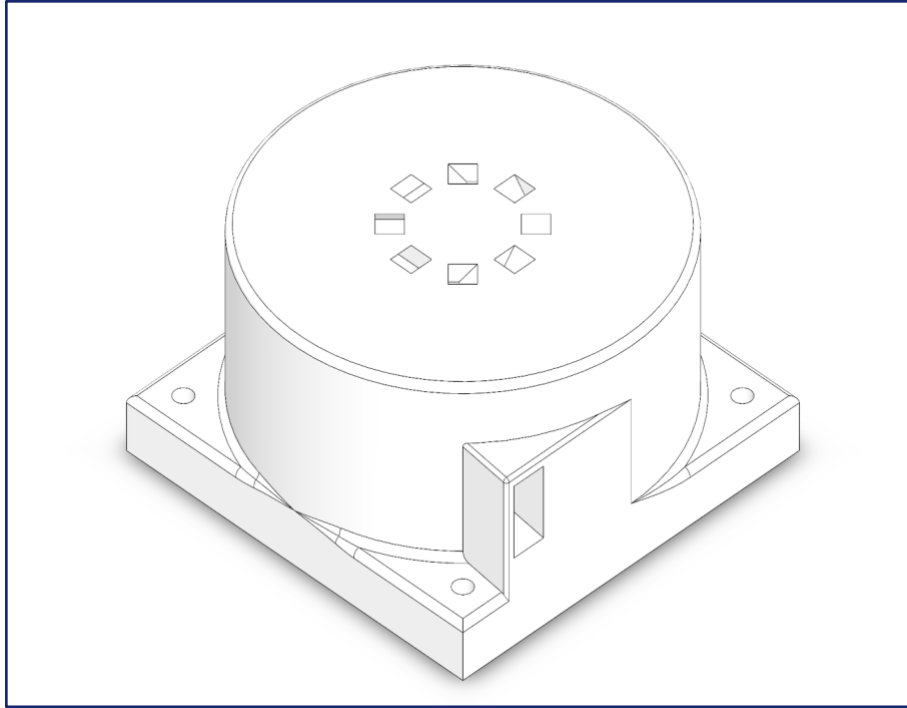
FIGURE 19: COVER MODEL WITH RPM SENSOR MOUNT

The sensor end uses a friction fit to stay firmly in place but can still be easily removed if desired. The four leads that were snipped to separate the sensor end from the rest of the chip were soldered back together to create a functioning sensor.

4.4 ATTACHING THE GYROSCOPE ONTO THE MOTOR SHAFT

When it comes to rotating objects, it is very important that they be balanced and securely fitted as exactly as possible. Errors in the balance and the shaft fitting will cause the gyroscope to oscillate and vibrate, making it loud, uncomfortable, and inefficient. To ensure that our gyroscope is fitted as tightly and accurately as possible, a shrink fit was determined to be the best way. A shrink fit uses the principles of thermodynamics to expand a piece of metal to a point where it can fit onto another, and then allowing it to cool on the piece so that it contracts and

creates an exact, tight fit. In order to do this, we did calculations on the thermal expansion of gyroscope with various shaft hole sizes based off of our motors shaft.

4.4.2 INTERFERENCE & FLYWHEEL STRESS

The team calculated the stress based off the shrink fit characteristics. For this calculation, the worst-case tolerance scenario used the maximum shaft diameter and the minimum bore diameter. As shown in the calculations in Appendix B, the interface pressure between the shaft and the bore in the disk was found to be 0.172MPA. From there, the stress of the bore on the disk and the shaft stress could be calculated. The bore stress is 337 MPa and the shaft stress is 0.172 MPa. This does not exceed the ultimate tensile nor the yield strength of the brass. The strain of the shaft was calculated and considered to be insignificant, whereas the strain on the bore was calculated to be about 0.008mm.

To ensure the brass disk did not fail under high rotation, the tensile stress of the outer rim was calculated using the density of the brass, the radius of the disk, and the maximum RPM of the motor. The tensile stress at the outside of the disk is 135 MPa. See Appendix B for full calculations.

5.0 FINAL PROTOTYPE

This chapter describes the final design after testing on the preliminary model was conducted. Each of the following subsections describe the main design iterations and adjustments each component underwent. At the end of this section, there will be a summary of the prototype in its final state.

5.1 CRADLE

The most important component that was added to the design is the cradle. The cradle is a component that rotates within the base and allows the gyroscope to precess. Initially, the cradle was designed as a simple swing with two support pillars. At the top of each of the pillar's holes were created to connect to rotating pins to allow the cradle to swing with the gyroscope's precession. The teamed then placed holes located in the center of the cradle to allow the motor to be mounted to the system by screws through the bottom. In this arrangement, the holes are aligned such that the wires for the motor exit out of the front of the cradle through the small rectangular channel. This can be seen in Figure 20 shown below.
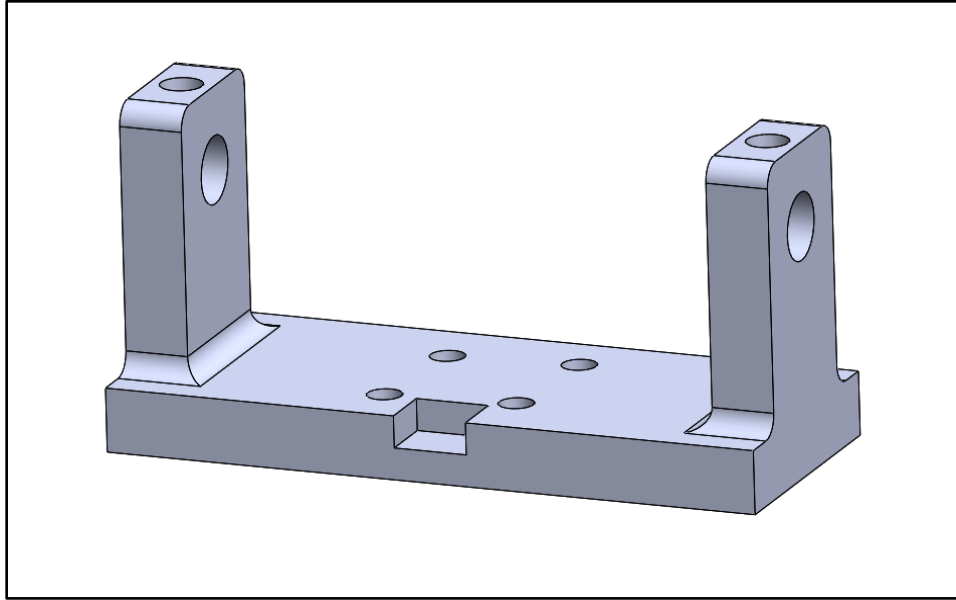
Upon assembling our first rendition of the cradle with the rest of the assembly, the team noticed that the wires coming out of the front caught on the base component and inhibited the cradle's ability to rotate freely. Another flaw in the design was that there was also no way to mount the RPM sensor to monitor the speed of the gyroscope. Lastly, the team noted that with the motor and gyroscope attached, the system became bottom heavy, which impeded the cradle's ability to rotate freely.

In order to solve these issues, the team needed to redesign the cradle from the ground up. The redesign began by creating a side view sketch of the system. The COM of the gyroscope was centered about the rotational axis of the cradle, thus ensuring that the system would be relatively balanced once assembled. There would be a slight imbalance due to the weight of the motor, but the team deemed this to be a beneficial feature that would help the cradle to return to an upright position naturally. An image of this sketch can be seen in Figure 21 below, in which the center point of the circle marks the placement of the COM of the gyroscope.
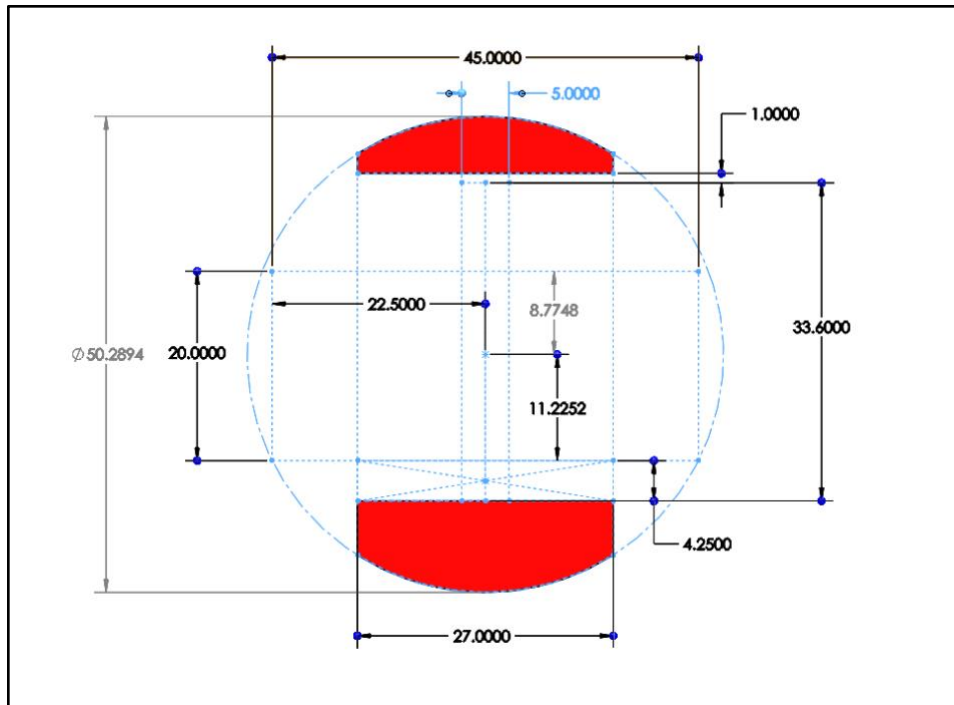
FIGURE 21: CRADLE SIDE VIEW SKETCH

The team figured that the best place to position the RPM sensor was above the gyroscope with the IR sensor looking down at the top surface of the gyroscope. This location was selected because it would keep the balance of the system located over the cradle's rotational axis and would prevent a bulky mounting bracket having to be made to fit and attach to the system. This turned the cradle from a simple U bracket shown in Figure 21 above, to a fully enclosed rectangular shape, which can be seen in Figure 22 below.

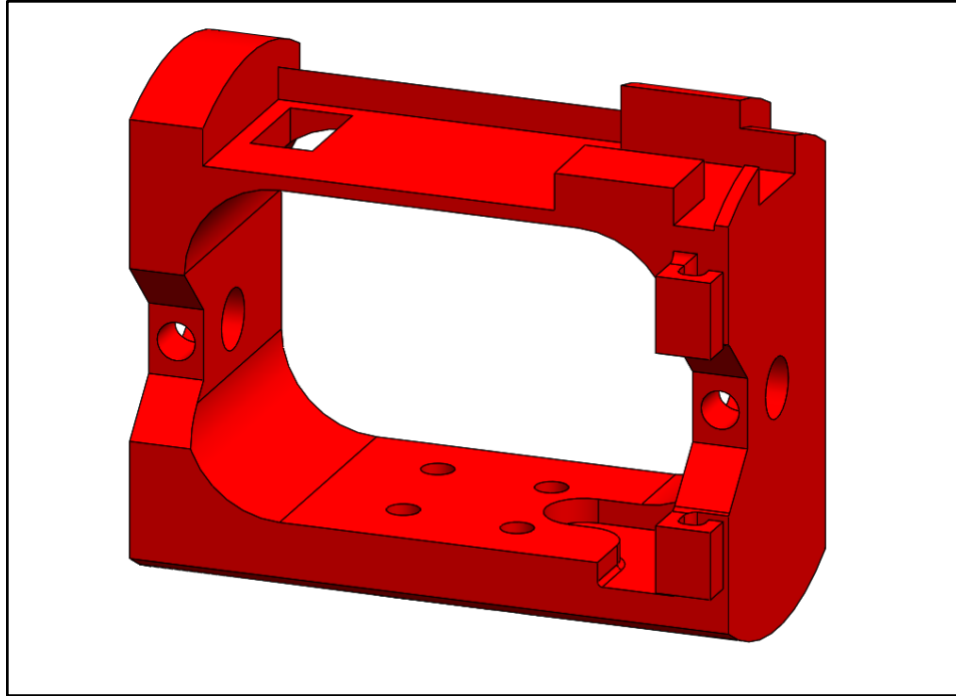The other significant change made to the cradle was the implementation of a wire management system for the motor wires. The motor mounts were rotated 90 degrees so that the wires come out in the center of the cradle floor. They then follow the channel around to the side of the cradle pillar and travel up the pillar through the two brackets. The wires then wrap around the top of the cradle and exit out the same side. To prevent the cradle spinning around on itself and binding up the wires, a built-in bumper system was designed in conjunction with the base to restrict the rotation of the cradle. This system consists of the extra extrusions on the top of the cradle, which also help to hold the RPM sensor and wires in place, along with features on the base which will be discussed in the following section.

The final adjustments made to the cradle consisted of making small edits to various features on the model. The entire frame of the model was shifted slightly to accommodate changes being made to the base. This decreased the thickness of the floor by about 2 mm, with the ceiling thickened by the same amount. The wire brackets on the cradle pillar were expanded

to allow for the motor wires to pack in more easily, as the previous ones were not wide enough. The final model of the cradle can be seen in Figure 23 below.
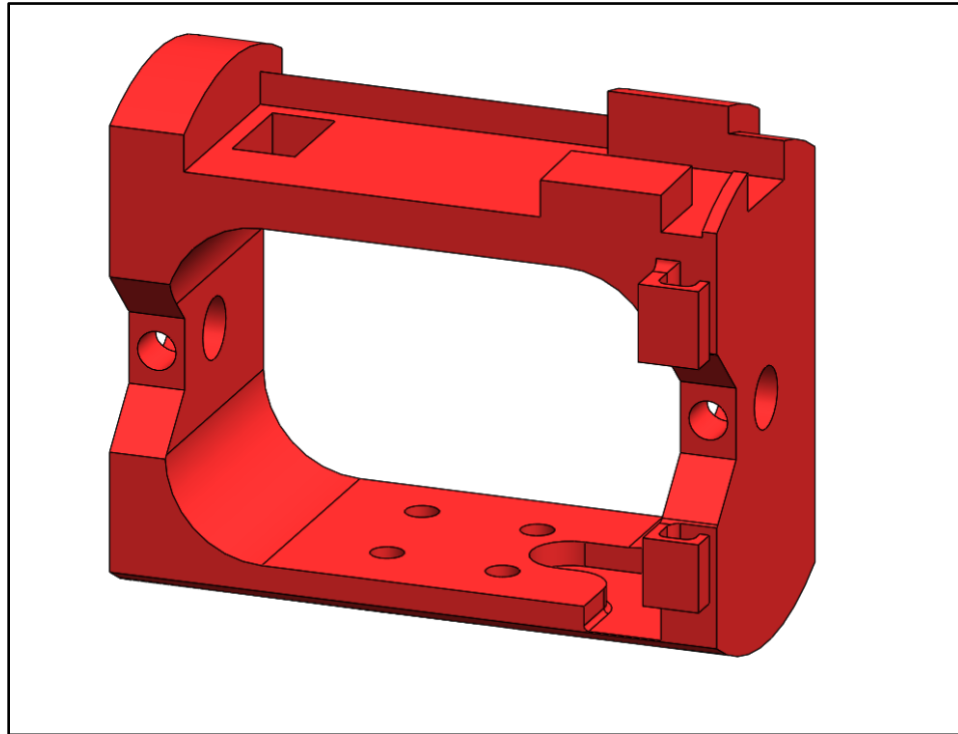
FIGURE 23: CRADLE FINAL VERSION

5.2 BASE

With the introduction of the cradle, the base also had to go through a series of design changes as well. We started by adding posts to the left and right sides of the wearer's hand to hold the cradle. The posts had spaces placed in the sides to hold a set of ball bearings in place via a press a fit. The ball bearings selected had an outer diameter of 0.625 inches, purchased from McMaster Carr (Item #: 60355K503). For each of these bearings, a pin was set through them to act pair of inline axles to allow the cradle to rotate freely. Since this was the first iteration introducing the cradle, the team was not yet concerned with an attachment method for a potential cover. The first design for the base in this design series can be found below in Figure 24.

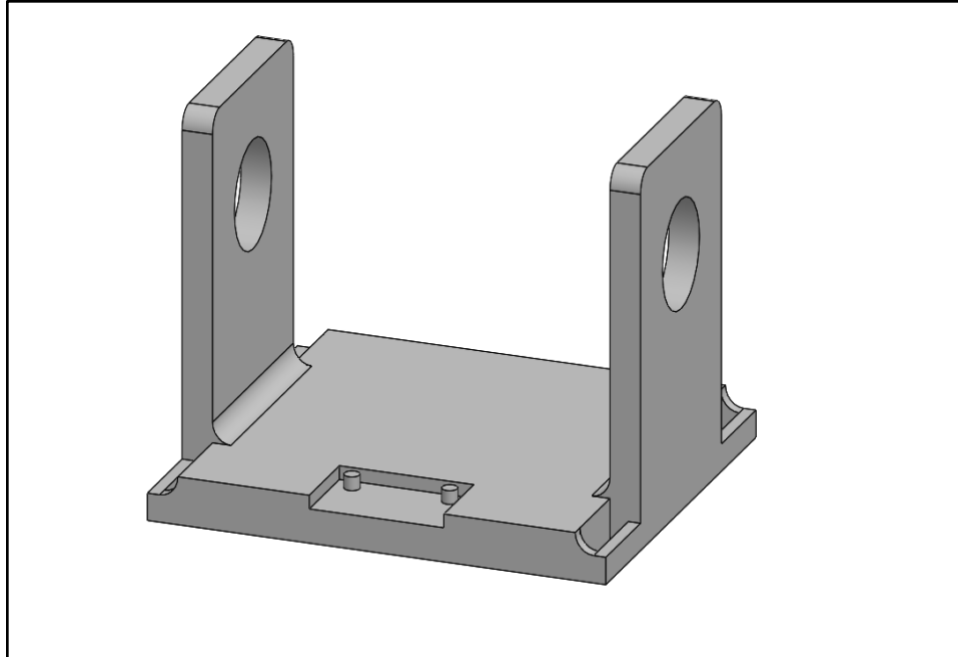When the necessary changes to the cradle were made, the team in turn had to make changes in conjunction with the base. The most significant change made to the base are the bumpers on either side of pillars. The addition of these bumpers restrict the rotational motion of the cradle to 90 degrees in either direction by interfering with the corresponding bump outs on the cradle discussed above in Section 5.1. This restriction allows for the cradle to remain in its effective range, as well as keep the wires from getting wrapped around the pins and getting caught between the base and cradle. In the next design iteration, the design was changed to fit a cover over the top of all of the moving parts. To allow the cover to attach to the base, 4mm holes with threaded inserts were added to the corners of the base. The tops of the posts were then rounded to fit the cover, described in the next section below. The second version of the base component can be seen below in Figure 25.
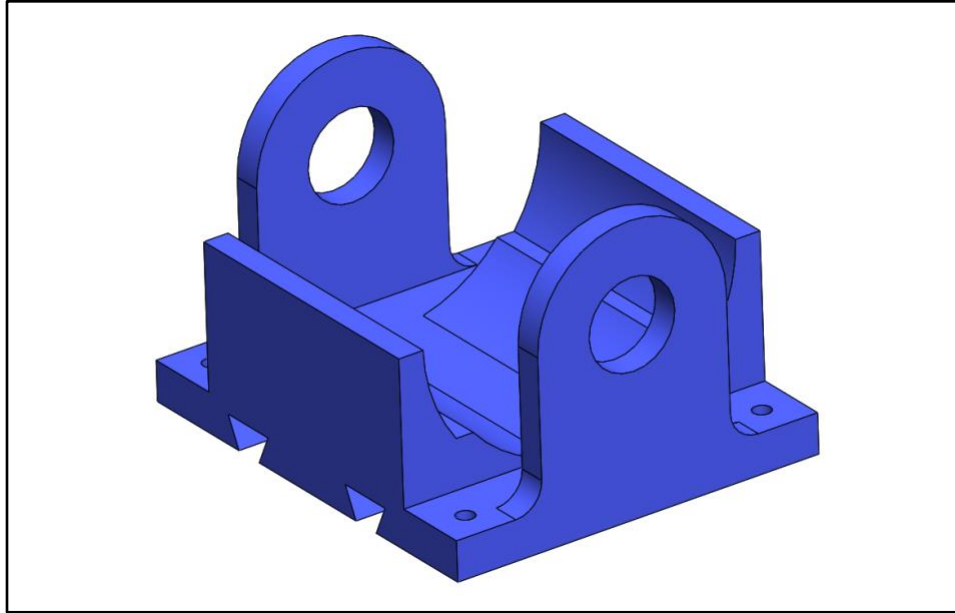
In order to make the base design fit comfortably on an individual's hand, the team decided an ergonomic fitting would have to be created on the bottom side of the casing. Rather than limit the device to only having the one ergonomic bottom, the team decided to make the bottom of the base modular. To do this, inverted trapezoidal channels were added to the bottom of the base through which matching groves on a customizable mounting plate can slide through to join the two components. This allows the device to be able to have multiple mounting surfaces on the bottom, including both test and ergonomic mounts. The mount will be covered further in Section 5.3. An image of the bottom of the base to show these channels more clearly can be seen in Figure 26.
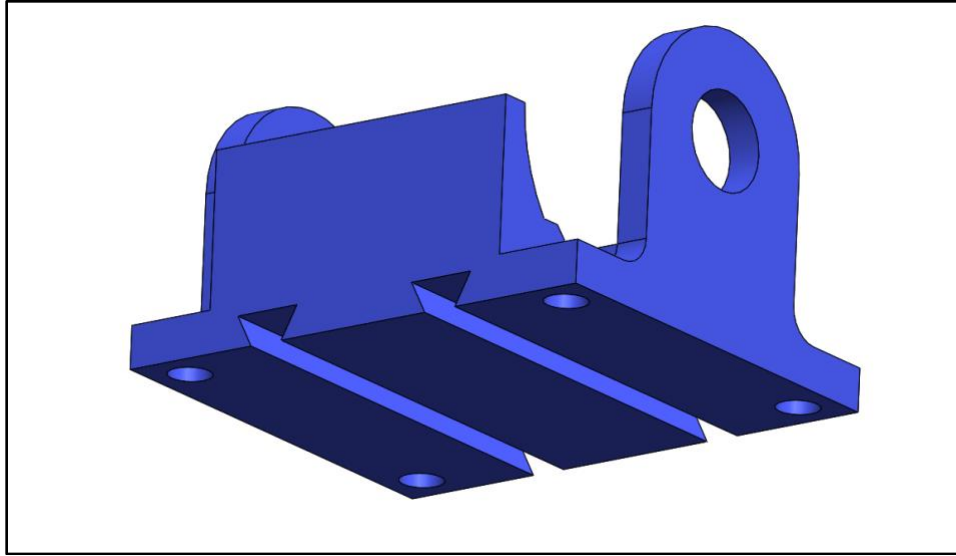
FIGURE 26: BASE VERSION 2.2 – UNDERSIDE

When the overall geometry had to be shifted again, this too corresponded to small changes made to the base model. The height of the side pillars was increased slightly, and the interior curve along the cradle's swing path was smoothed out to prevent any contact by the bottom of the cradle. In an effort to join both the base and hand mount, it was initially difficult to get the two to slide easily together. For this reason. The dimensions of the channels were adjusted to allow for more of a sliding fit, and the openings of the channels were filleted for easier alignment of the two components. The bumpers were also raised by 10 degrees, to restrict the cradle by +/- 80 degrees in either direction. This was done because during the first rounds of testing with base 2.2, the cradle would occasionally get stuck in the maximum positions, and have a difficult time returning to center. The final model of the base component can be seen in Figure 27 below.
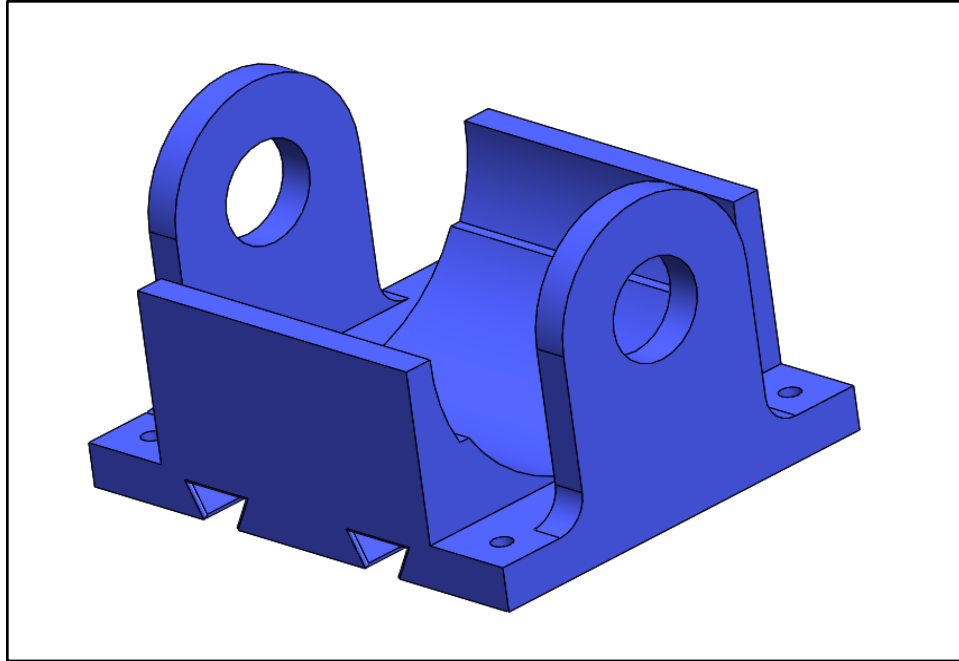
5.3 HAND MOUNT

The purpose of the hand mount is to provide a comfortable way for the device to be mounted on a hand as securely as possible. It is important that the mounting surface be comfortable, because if it isn't the user will not want to wear it. The device also needs to be securely attached to the hand because this has a direct impact on the effectiveness of the device. If it is allowed to shift and slide, the device will not be able to react properly to the movements of the hand.

The team first created a mounting plate that could be attached to the modular body. By creating an inverted trapezoidal extended feature, the mounting plate can slide into the channels on the body to provide a flat bottom to the device. The four loops on the sides of the mount are to allow for Velcro straps to attach the device to the hand. This plate, shown below as Figure 28, was used during testing to provide a flat surface to make attachment to the testing apparatus

more effective. This mounting plate was then used as a base model for the ergonomic hand mount.
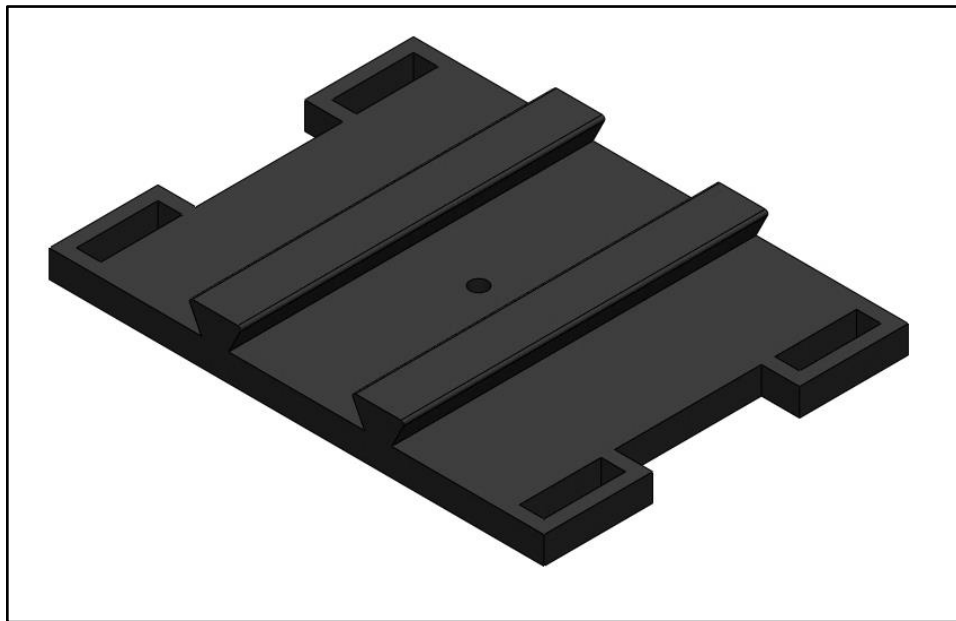
FIGURE 28: BASE MOUNT

When designing the hand mount, the team decided that the most effective method would be a design that fits the surface of the average hand as accurately as possible. A 3D model of a male's left hand was found on the design community page "GrabCAD" and used as a surface geometry reference. The hand was inserted into the base mount file and located to a reference position below the base mount, as can be seen in Figure 29 below.
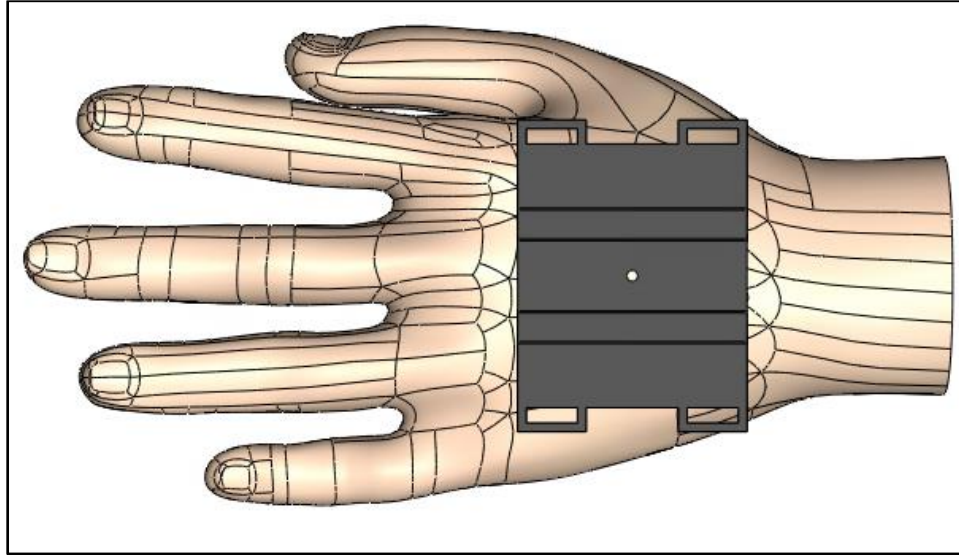
The team extruded the bottom surface of the base mount down to match the top surface of the hand model. This created a solid, exact connection between the hand and the mount. The edges of this extrusion were then filleted to increase comfort. The initial design of the hand mount was created based on an average male's hand, but the scaling of the hand mount can be customized, therefore allowing the device to fit 95% of hand sizes. The final hand mount design can be seen below in Figure 30.
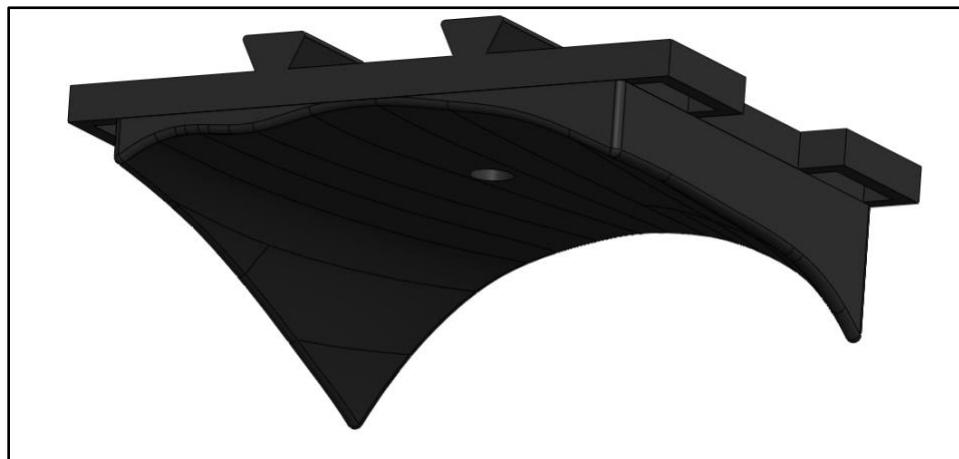
FIGURE 30: FINAL ERGONOMIC HAND MOUNT

With the new base and cradle system in place, there was now less room in between the pillars of the cradle for the original gyroscope to fit. With these new constraints, the dimensions of the gyroscope had to be altered to fit the new arrangement. The overall diameter of the gyroscope was decreased to 45 mm across, thereby creating 2 mm on either side between the gyroscope and cradle pillars. A model of the gyroscope can be seen in Figure 31 below.
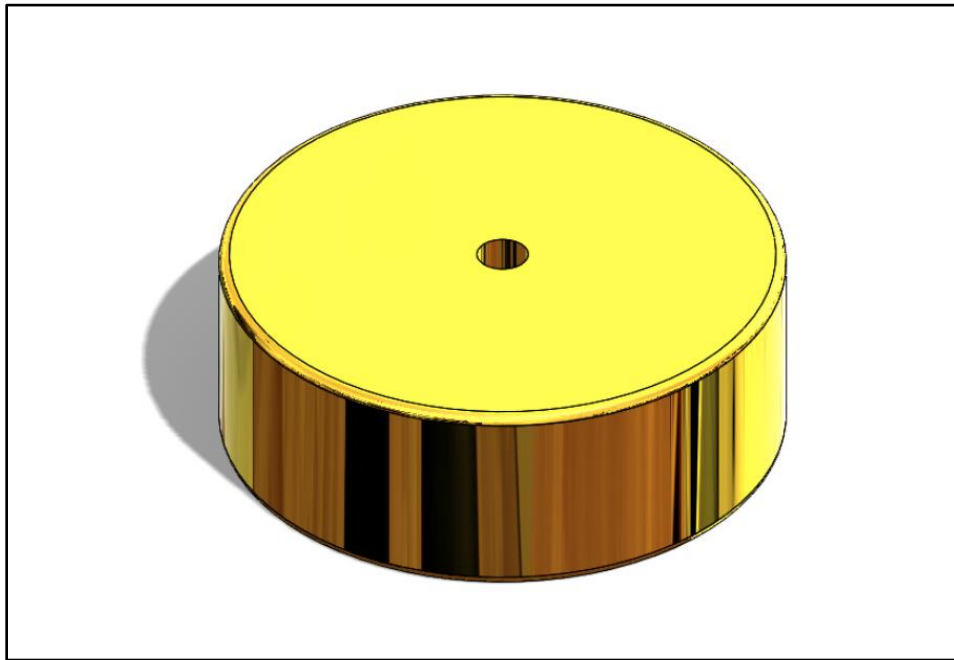
FIGURE 31: GYROSCOPE FINAL VERSION

Using the procedure lined out in Section 4.4.1, the team was unable to achieve the desired shrink fit due to the gyroscope not fitting over the shaft. Two attempts were conducted using a gyroscope with a shaft hole size of 4.93 mm. After conducting our procedure, the team discovered that either the measured the dimensions of the motor were incorrect, or there was not enough clearance between the motor shaft and gyroscope, because once the gyroscope was heated, it did not slide onto the motor as intended. These attempts resulted in the bending of the motor shaft, making it unusable. For the final disk, the hole was expanded to 4.95 mm to match

the size of the shaft, and a new motor was purchased. From previous testing, this type of fit

worked well on the motor and did not cause any issues. The resulting fit was snug and fit over

the shaft.

5.5 COVER

With the completely redesigned base and the addition of the cradle, a new cover needed

to be designed to encase all of the internal components. The cover was designed to fit starting

with the second iteration of the base, base 2.2. The main cavity of the cover provides enough

room for the cradle to swing freely and is toleranced to slide onto the base with ease. On one side

of the cover is a slot that allows for the wires from the cradle to exit the device. The slot travels a

full 180 degrees around the top of the to follow the motion of the cradle. The first design of the

cover can be seen below in Figure 32.
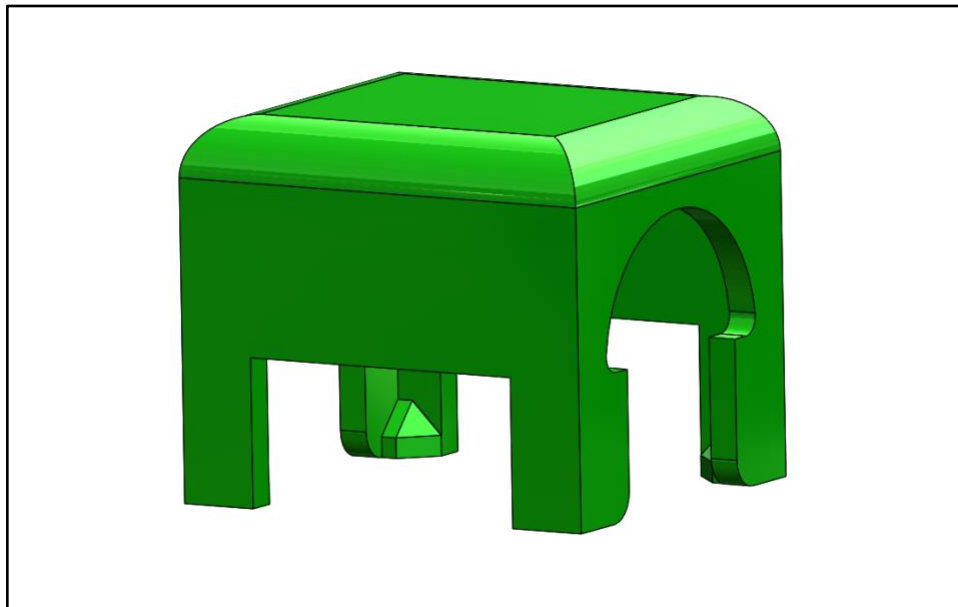
FIGURE 32: COVER VERSION 2.2

To attach the cover to the base, 4mm holes were placed in the bottom of each of the feet.

These holes then had 3mm brass threaded inserts press into them. These holes match up with

holes on the base for 3MM screws to come through and secure the cover in place. These can be seen below in Figure 33.
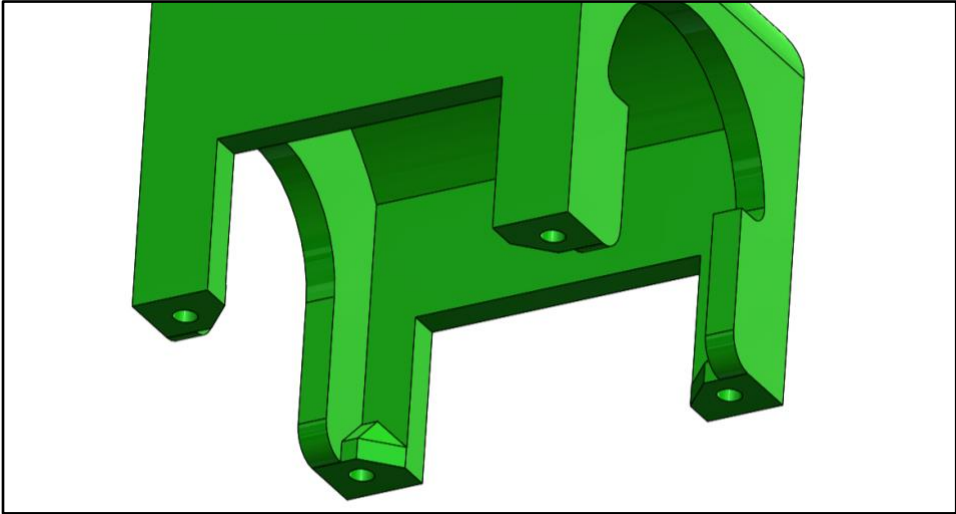
FIGURE 33: COVER VERSION 2.2 – UNDERSIDE

The second version of the cover features a rounded roof that reduces the amount of material used. The slot around the base pillar was also increased to go lower on the cover to reduce some of the dragging the wires were experiencing with the previous model. The final model of the cover can be seen in Figure 34 below.
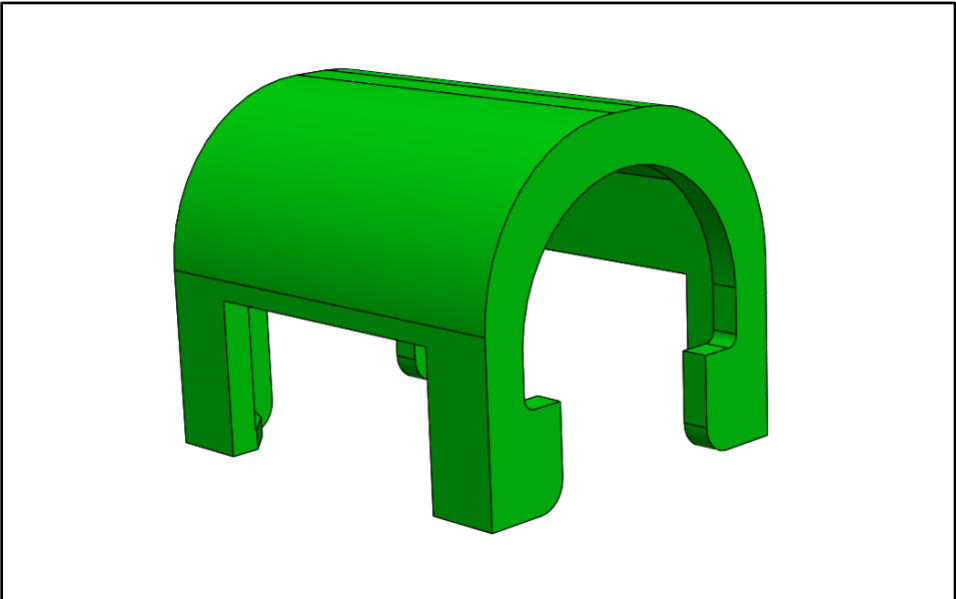
FIGURE 34: COVER FINAL VERSION

The components described above, with the exception of the gyroscope, which was machined on a lathe, were all manufactured via a 3D printer with PLA plastic. The parts were printed using a 35% infill and 1.4 mm wall thickness to give the parts enough strength to hold the other components in place. Seen below in figure 35 is an exploded view of the final assembly with all of the components and fasteners.
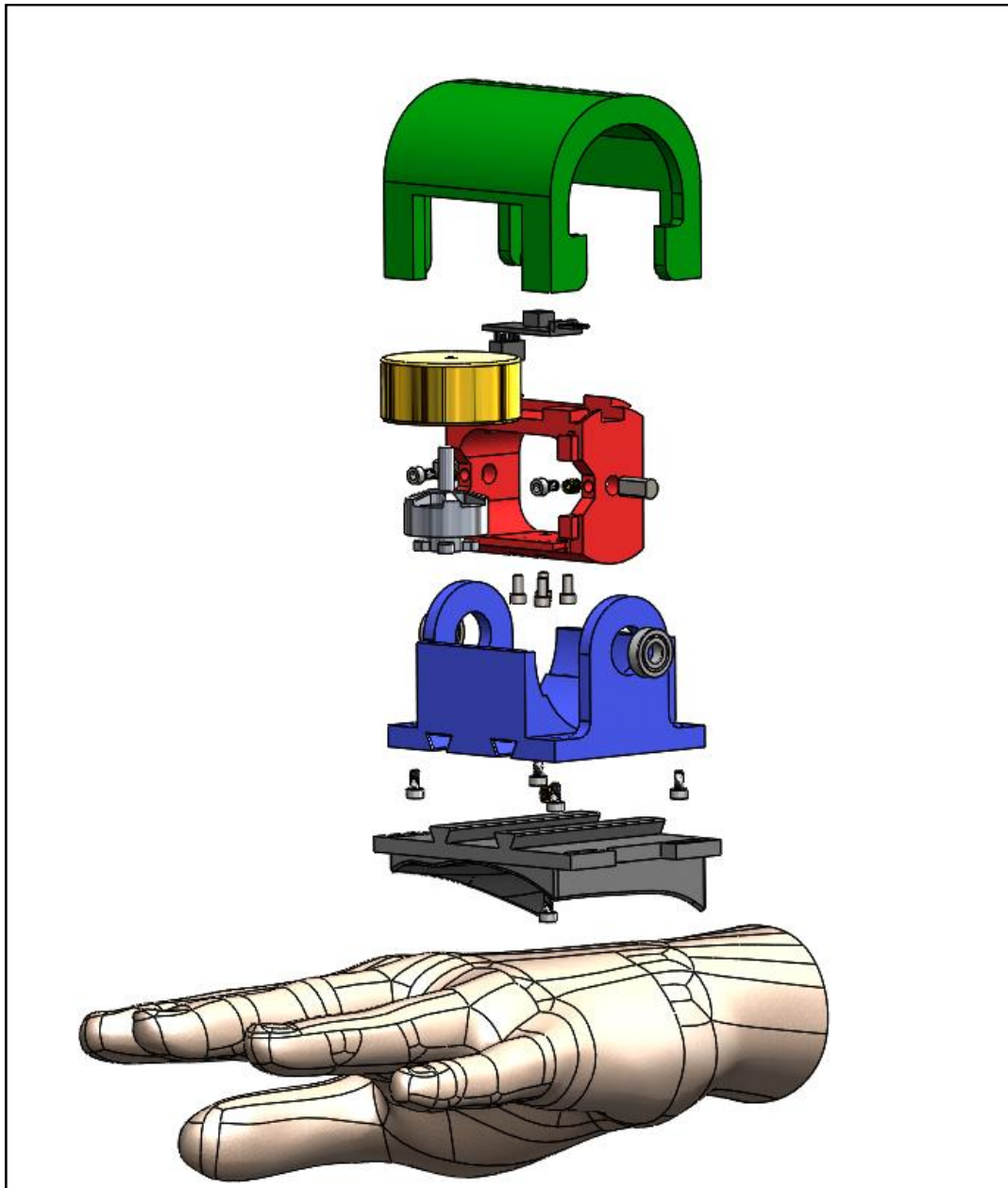
FIGURE 35: EXPLODED VIEW OF FINAL ASSEMBLY

Figure 36 below shows a top view of the device with the cover removed. Mounted on top of the cradle is the RPM sensor chip glued in place to reduce any vibration. The wires from the motor come up the cradle on the right side through the brackets and exit the device on the cradle's top surface. The wires are secured further with electrical tape to ensure they do not come free of brackets.
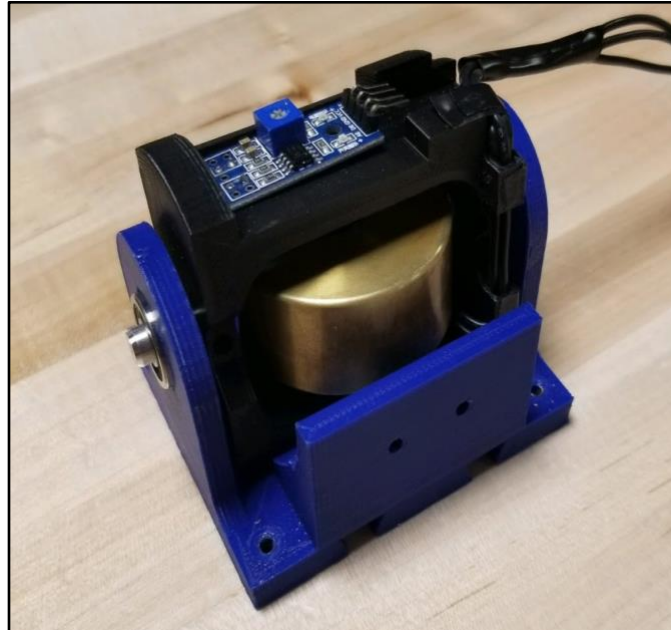
FIGURE 36: ASSEMBLY WITHOUT COVER AND HAND MOUNT

Figure 37 shows the device attached to a hand using the hand mount and Velcro straps, again without the cover. Here it can be seen how the contours of the hand mount follow that of a hand to create as comfortable as fit as possible. As stated before, the hand mount platform can be custom fit to 95% of hands. The ball bearings and axle pins can also be seen assembled on the base pillar.

FIGURE 37: ASSEMBLY ON HAND WITHOUT COVER

Figure 38 shows the fully assembled device mounted to the hand. This image clearly shows how the wires exit the internal area and can freely rotate with the cradle through the length of the slot.

FIGURE 38: FULL ASSEMBLY ON HAND

6.0 RESULTS

This chapter discusses the process used to evaluate the prototype and analyze the collected results. The first section discusses purpose and reasoning for the testing used, followed by a discussion regarding those results and the analyses carried out.

6.1 LEVER ARM TEST DESIGN

To quantify the effectiveness of the device, the team decided to create a test to observe the reduction in rotational motion. As discussed in the background, tremor can be assimilated into a sinusoidal wave, which is characterized by two main factors: frequency and amplitude. The gyroscopic effect reduces the amplitude of the user's tremor without impacting the tremor frequency. This means that although the device does not have a direct impact on the time of the tremor impulse, it does reduce the displacement of rotational motion in that time.

To imitate a single motion of a tremor, a pendulum or lever arm with the device attached to the end was used to observe the reduction in swing time of the lever arm. The lever arm geometry is fixed and was assumed to have frictionless bearings to rotate about. The independent variables were the RPM of the gyroscope, the angular displacement of the lever arm, and the initial position of the cradle. The hypothesis was that the swing time of the lever arm would increase as the RPM of the gyroscope was increased. The test measured the swing time of the lever arm, with measurements taking at a range of motor speeds and swing starting angles. By calculating the percentage increase in swing time of the lever arm, the percent reduction in tremor motion could be determined.

To do this, the team conducted testing and analysis in both theory and practice. Using information on the amplitude and frequency of Essential Tremor, the most common tremor disorder, the team determined important numerical factors such as the degrees of rotation caused by tremor motion, angular velocity and acceleration of the tremor, and frequency of motion. These numbers were referenced for creating an accurate model that described the summation of the forces during the use of the team's device. The mathematical model shown in Section 2.6 was used for these calculations. The complete model can also be seen in Appendix E. For the practical testing, the team used the lever arm experiment stated above.

In the lever arm test, a high-speed camera was used to capture the swing duration of the lever arm at various angular displacements. For displacements of 5, 10 and 15 degrees, three trials were conducted with the gyroscope at a constant speed of 0, 6000, 10000, 140000, and 18000 RPM. The footage was then analyzed to determine the time the lever arm took to fall from its set angular displacement to 0 degrees. The average of these times were then used to compare the time of the freefall swing and determine the percent increase in swing time. A step by step procedure of the lever arm experiment is located in Appendix D.

6.2 FULL CRADLE ROTATION TEST

The initial testing conducted had the cradle positioned to the left in a maximum -90-degree rotation. This allowed the cradle to have a full 180 degrees to rotate. For this test, the Casio EXILIM high speed camera was used to capture the motion of the lever arm. Due to the hardware limitation of the camera, the 239.76 frame per second footage was converted to a playback speed of 29.97 frame per second (fps). Therefore, a time conversion was required to convert the playback speed to real time. The proportion was calculated to be one second of

239.76 fps video was equivalent to 8 seconds of playback in 29.97 fps footage. The Movavi

video editor was used to obtain the timestamp of the initial and final angle of the lever arm.

Below in Figure 39 are the results of the full rotation test.
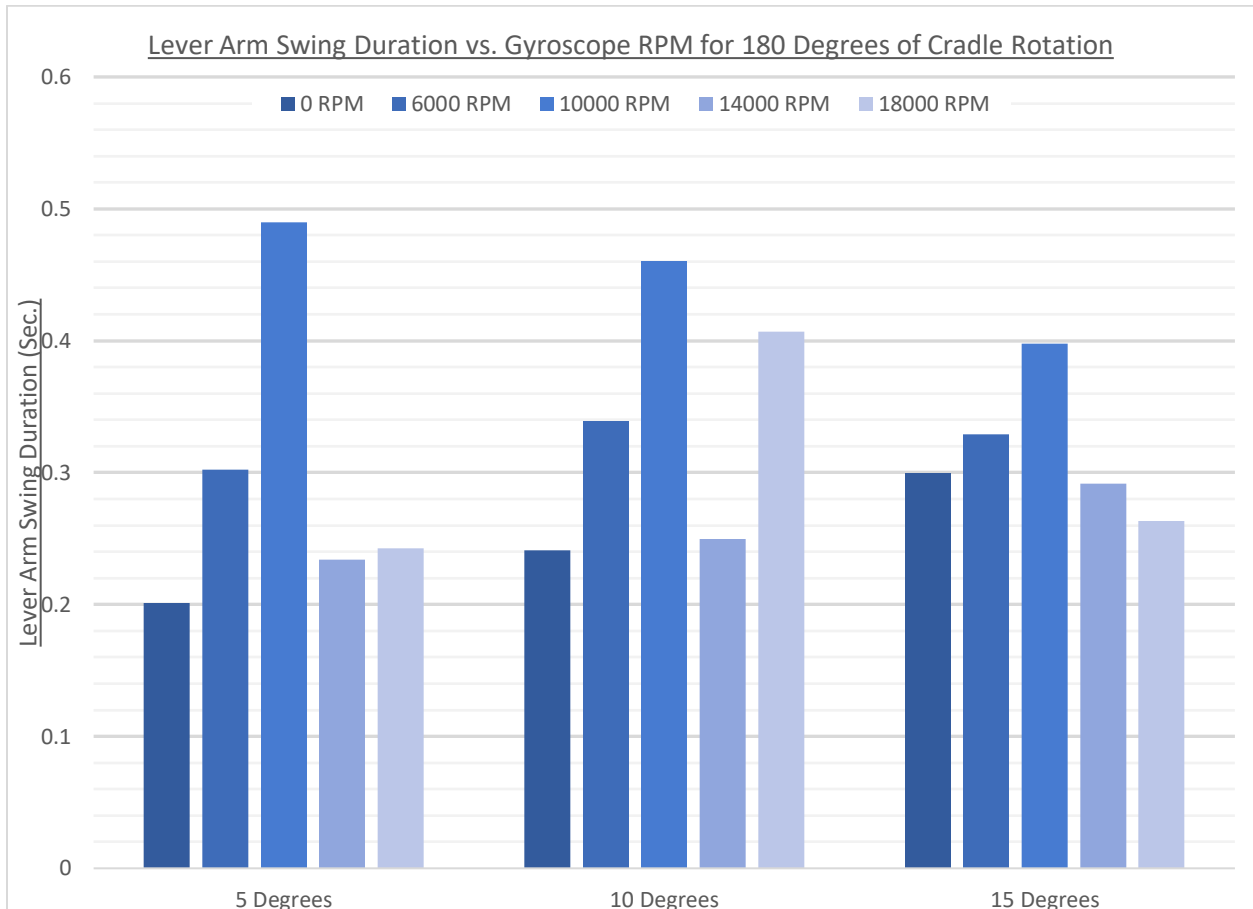
FIGURE 39: LEVER ARM SWING DURATION VS. GYROSCOPE RPM FOR 180 DEG. OF CRADLE ROTATION

The raw data can be found in the Appendix G. For the first set of data at 5 degrees, the

time of freefall of the lever arm is the shortest at 0.2 seconds. When the gyroscope was spun to

6000 RPM, a 50% increase in swing time was computed. At 10,000 RPM, the increase in time of

swing was approximately 143%. However, at 14,000 and 18,000 RPM, the percent increase is

16% and 21% respectively. In the second set of data of 10 degrees, the freefall time was 0.24

seconds. The percent increase in time was 40% at 6000 RPM, 90% at 10,000 RPM, 4% at 14,000

RPM, and 69% at 18,000 RPM. In the third set of data at 15 degrees, the freefall time was 0.3

seconds. The percent increase at 6000 RPM was 10%, at 10,000 RPM was 33%, at 14,000 RPM was 3%, and at 18,000 RPM was 12%.

It is evident in this relationship that the increase in RPM increased the swing time of the lever arm. This is visible for all initial angle sets at 6000 and 10,000 RPM. This proved our hypothesis and the simulation in the mathematical model. Additionally, it was also observed the percent increase diminishes as the angular displacement of the lever arm grew from 5 to 15 degrees. However, a point of error was denoted in the data sets at an RPM of 14,000 and 18,000. The team observed that the gyroscope had an effect on the period of the lever arm, but this effect occurred after the lever arm had passed through the determined end point of 0 degrees. The gyroscope was also observed to not react instantly to the motion of the swing. In the footage of 14,000 and 18,000 RPM, the cradle was seen to rotate after the lever arm passed 0 degrees. The results show the error as swing times were similar to the original freefall time where the gyroscope was disabled.

The team believes that the reasoning as to why the gyroscope did not react in time was due to the initial angle of the cradle. With the cradle set at the -90 degrees to allow for the full 180 degrees of rotation, the gyroscope was taken out of its effective range, where the motion of the lever arm would not have a real effect on the motion of the cradle. The team then hypothesized the device would react immediately if the cradle's starting angle was set to 0 degrees. This decreases the overall allowed rotation of the cradle, however, would allow the gyroscope to rotate instantly at the start of the swing. This second test is discussed further below in Section 6.3.

6.3 HALF CRADLE ROTATION TEST

Following through on the team's reviews from the first lever arm test, the test was repeated in full, this time with the cradle oriented at 0 degrees at the start of the swing. The cradle oriented in this position, the prototype's resistive effects would be taking place instantaneously, compared to the previous test. For this test, the team switched to the GoPro 7 video camera to capture the lever arm motion. The advantage of the GoPro over the Casio EXILIM was the higher resolution of 1080p at the same frame rate. Additionally, the footage was saved in real time, so no time conversion was needed as in first experiment. Adobe Premiere Pro was used to view the footage because it was successfully able to open the video files and had the ability to scrub through the timeline accurately. The swing time was calculated using the reciprocal of 239.76 fps to find the time displayed per frame and multiplied by the number of frames. Assuming a constant framerate, one frame displays for 0.00417 seconds. The swing time results for the second test are shown below in Figure 40.
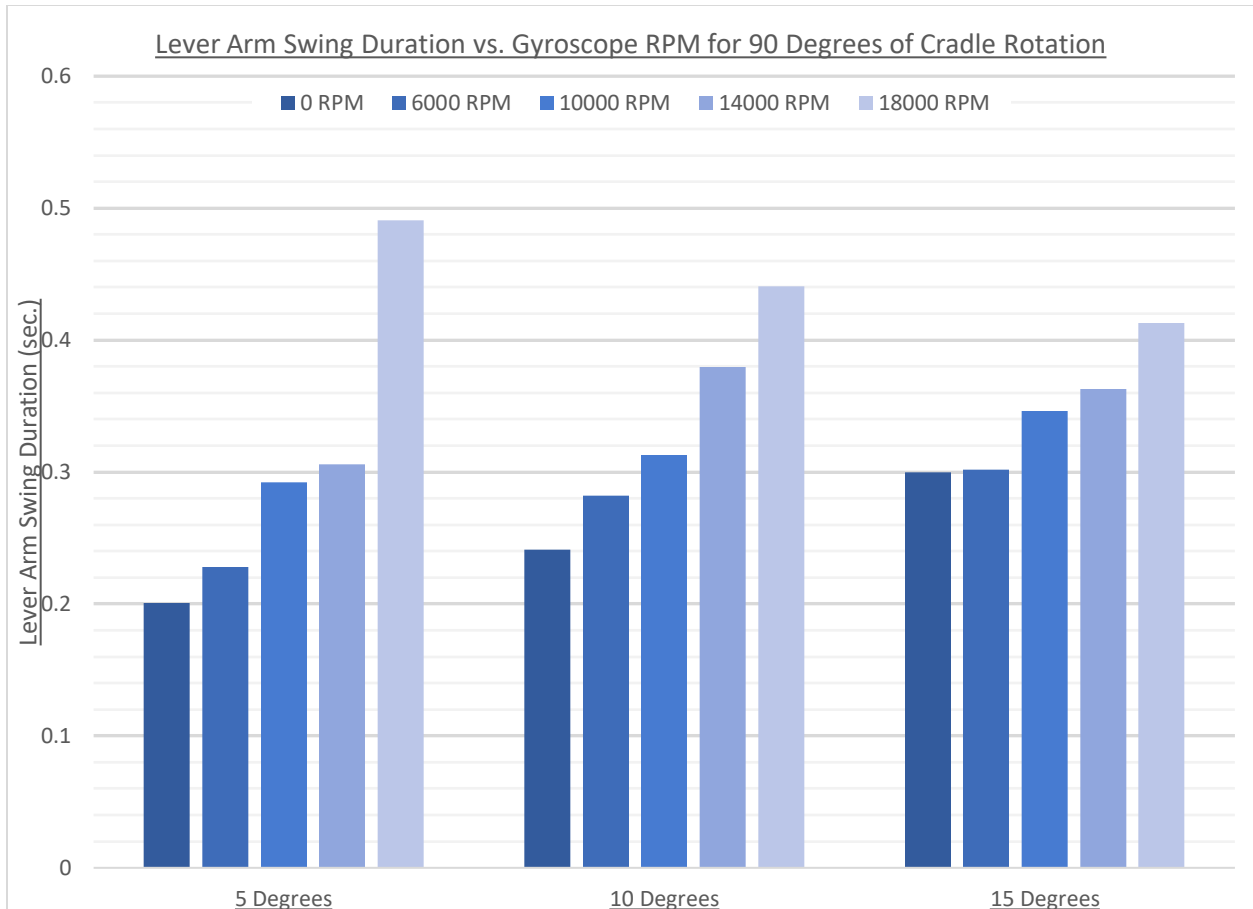
FIGURE 40: LEVER ARM SWING DURATION VS. GYROSCOPE RPM FOR 90 DEGREES CRADLE ROTATION

The raw data can be found in the Appendix G. For the 5-degree trials, the freefall time at 0 RPM was the same at 0.2 seconds. The percent increase at 6000 RPM was 14%. At 10,000 RPM the time increased by 45%. The time increased by 52% at 14,000 RPM. The final swing time saw an improvement of 144% at 18,000 RPM. In the 10-degree trials, the freefall time was 0.24 seconds. The percent increase at 6, 10, 14, and 18,000 RPM was 17%, 30%, 57%, and 83% respectively. The freefall time was 0.3 seconds for the 15-degree trial. The percent increase at 6, 10, 14, and 18,000 RPM was 1%, 15%, 21%, and 37% respectively.

Changing the initial cradle angle allowed for a quicker reaction from the gyroscope. This improved the data results for 14000 and 18000 RPM trials because the gyroscope was able to react within the testing measurements. Therefore, the team's second hypothesis was proven

correct. Following the first hypothesis, the increased RPM of the gyroscope does have a direct relationship with the swing time of the lever arm. The swing time positively increases due to an increase in the RPM of the gyroscope. While there is still an increase in swing time, the percent increase decreases as the starting angle of the lever arm is raised.

One observation of the 5-degree data set at 18,000 RPM is that the time increase was at 144%. However, the previous RPM saw an increase of 52%. The sudden jump in percentage was noted as an error in measurement since for the 10 degree and 15-degree trial, the time increase was linear whereas the time in the 5 degree was an exponential. Therefore the 144% was neglected as an error in measurement and the greatest reduction in time was in the 83% of the 10-degree data set.

The results from the second test were plotted individually for each angular displacement. Figure 41 below shows the data of the 5-degree test in detail. A linear fit was added to show the relationship between increasing the RPM and the time of the lever arm swing. The coefficient of determination, R^2, is also shown in the legend. The closer the R^2 value is to 1, the better the linear relationship. In the 5-degree test, the linear fit is drawn as the line $y = 0.0658x + 0.1063$, with an R^2 equal to 0.841 or 84.1%.
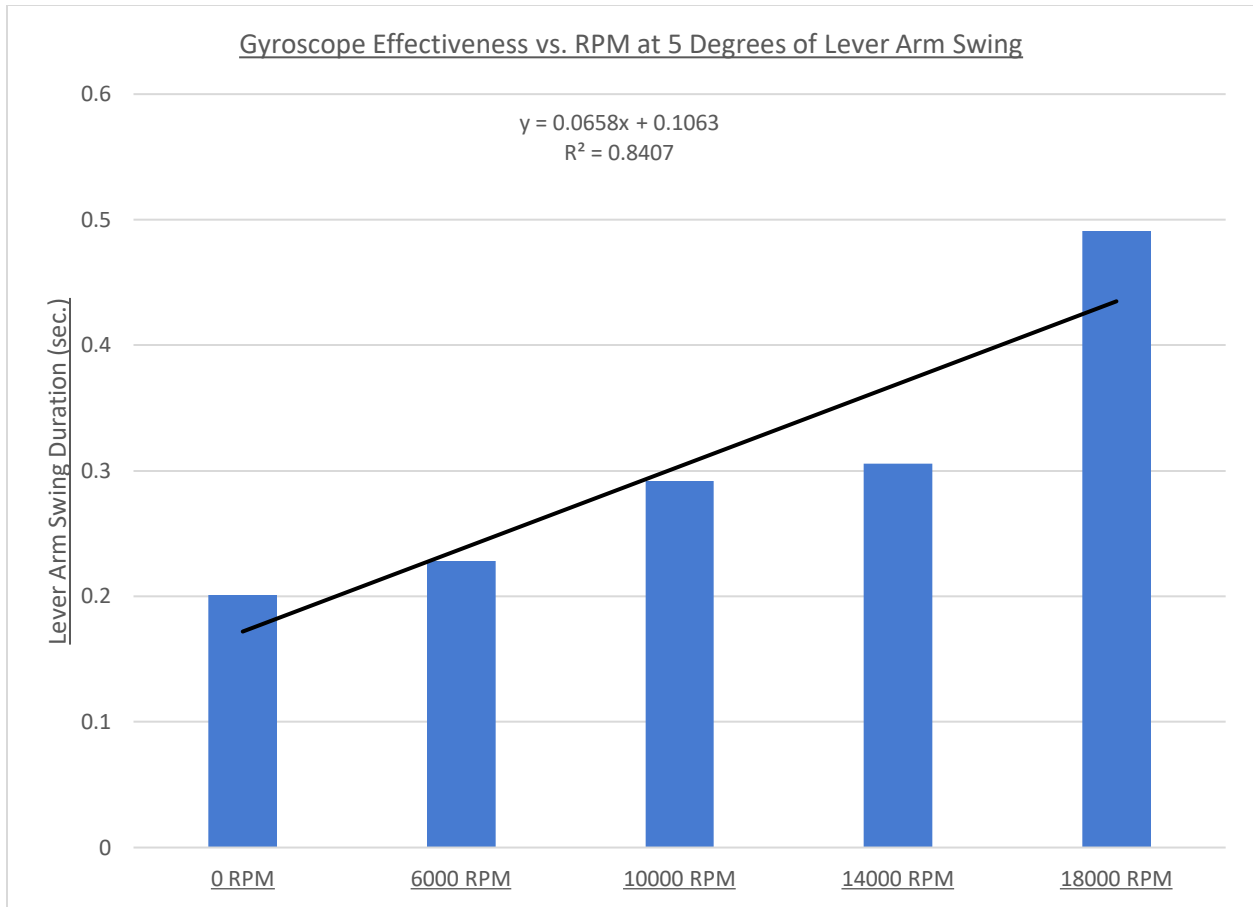
FIGURE 41: 5 DEGREE TEST DATA WITH LINE OF BEST FIT

This process was repeated for the 10 degree and 15-degree trials. The 10-degree angular displacement has an equation of $y = 0.0496x + 0.232$, with an R^2 value of 0.979 (98%). The 15-degree angular displacement has an equation of $y = 0.0287x + 0.287$, with an R^2 value of 0.933 (93%). The slope of the relationship between RPM and time was taken and plotted against the angular displacement.

An observation from the results was that increasing the angular displacement decreased the effect of the gyroscope acting on the lever arm. In Figure 42 below, the slope of the RPM relationship was plotted against the displacement angle in degrees. As the slope decreases to zero, the effectiveness of the gyroscope would fail to affect the time of the swing regardless of the gyroscope speed. The equation of the linear fit is $y = -3.71*10^{-3} x + 0.0851$. Extrapolating

the best fit line to the x-axis would give the angle where the device would have negligible or no

effect on the time of the lever arm swing. This angle was found to be about 23 degrees.
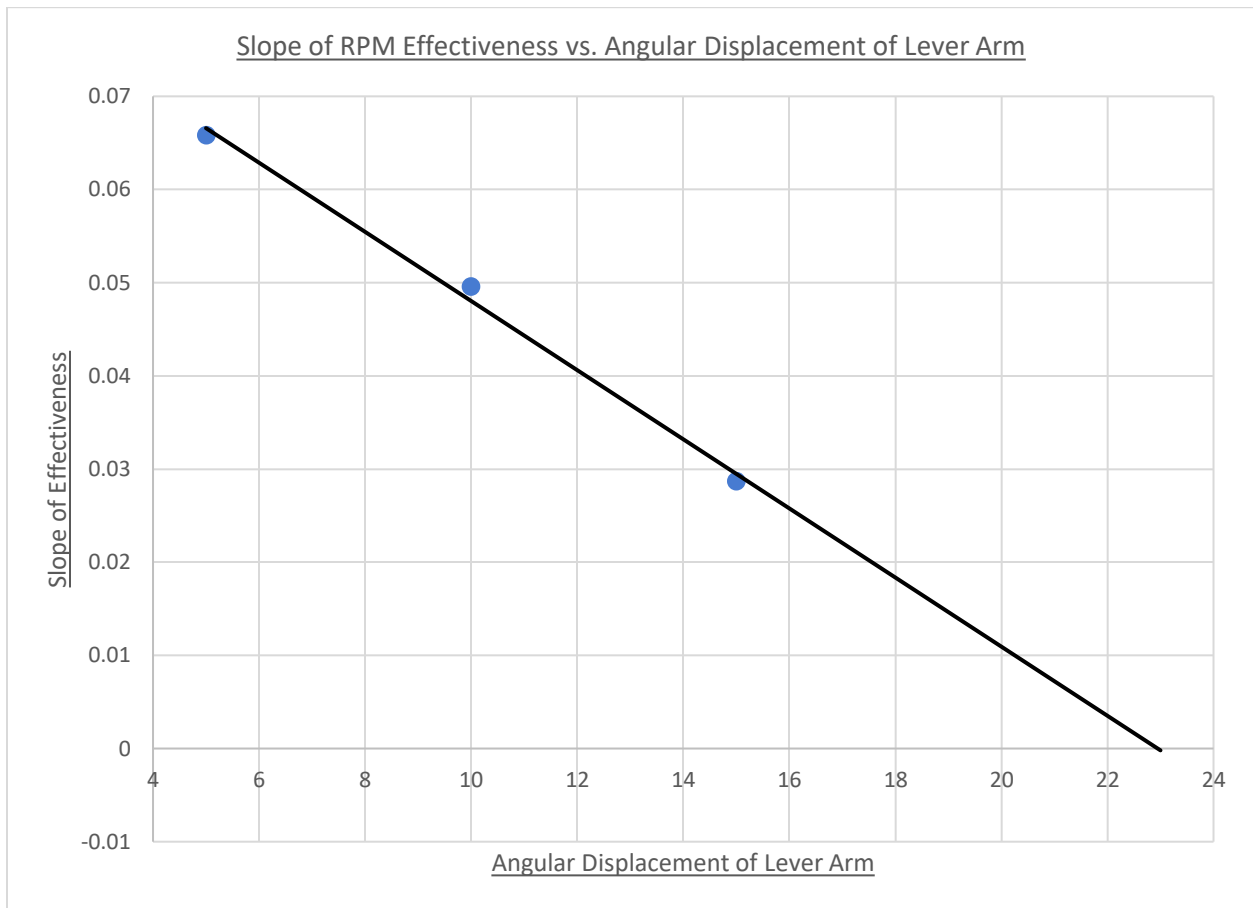
FIGURE 42: SLOPE OF RPM EFFECTIVENESS VS. ANGULAR DISPLACEMENT OF LEVER ARM

6.4 DISCUSSION

From testing, it was established that the team's hypothesis that the time increased as the

RPM increased was correct. Additionally, the effect of the RPM diminishes as the angular

displacement increased from 5 to 15 degrees. What we can conclude is the effectiveness of the

RPM on the reduction of the swing time in the lever test depends on angular displacement of the

tremor. Using the extrapolated information of the RPM effectiveness vs Angular Displacement

in Figure #2, we can conclude that for our lever arm setup, the maximum RPM effectiveness is at very small angles and the angle when the RPM has no effect on the swing of the is at 23 degrees. What this means for a tremor is that the device is very efficient in reducing tremor amplitude in rotational angles of 0 to 10 degrees. However, at 10 to 23 degrees, the efficiency decreases. To increase the effectiveness, a higher RPM is required, however that may be exponentially higher to achieve the same effect.

6.5 SIMULATION TEST DESIGN

During the course of testing, the team came up with a second method that could be used to test the effectiveness of the device. Using a linear actuator that acted at the same amplitude and frequency of a hand tremor, the team speculated a device that could actively recreate the conditions of a tremor. The device would consist of a flat piece of wood, the width of which being the average width of a male's hand, would be suspended along its length about 6 inches from the ground between two posts, each with an axle and bearing to connect them and allow the wood platform to pivot. A linear actuator, tuned to produce the same frequency, force, and displacement of a hand tremor (based on angular displacement and the width of the wood), would then be mounted below the platform and attached to one of the edges.   When the linear actuator is activated, it would cause the wood platform to oscillate at the same frequency and amplitude of a hand tremor. The team would then be able to attach the prototype to the platform and observe how the device interacted with the tremor. Figure 43 below shows a model of what the device would look like, and a full procedure for this can be seen in Appendix H. Unfortunately, due to time constraints, this second device could not be built.
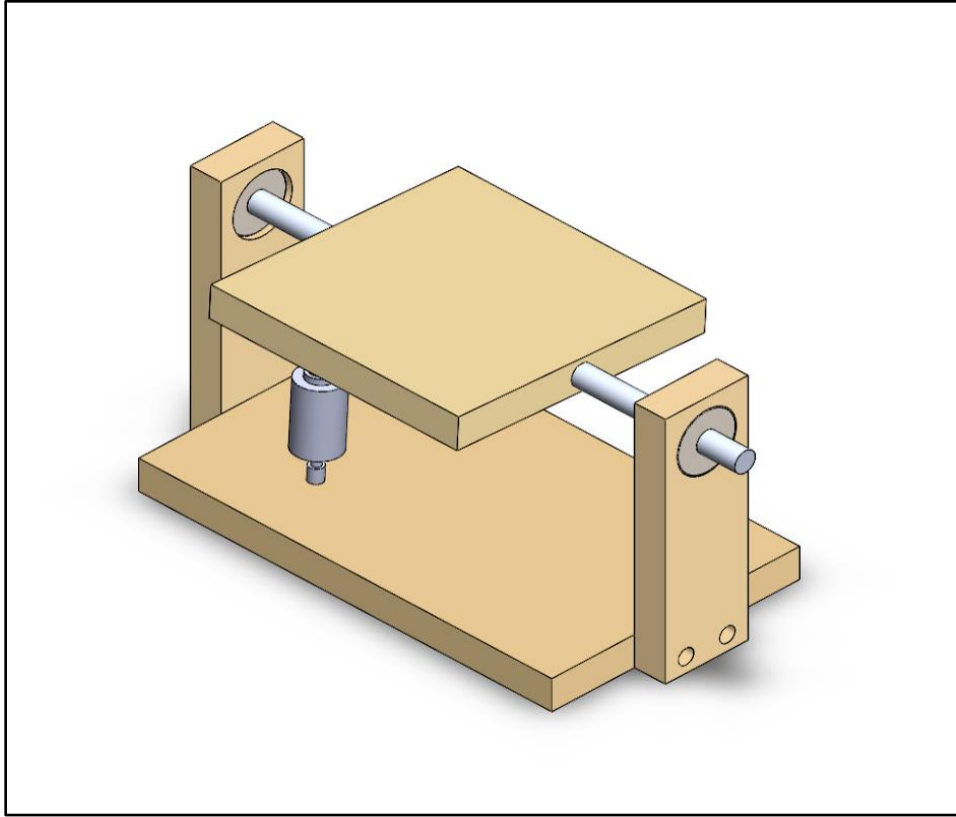
FIGURE 43: SIMULATOR TEST RIG DESIGN

7.0 RECOMMENDATIONS & CONCLUSIONS

Upon completion of this project, there are a number of recommendations that the group would recommend be taken given more time to continue development of the prototype.

1. Shrink components: Currently, the device is bulky to wear, and the electrical components are contained within a large acrylic box. Since the structure was manufactured out of 3D printed PLA plastic, a certain thickness had to be incorporated to ensure structural rigidity of the components, and thus increasing the dimensions. If the base, cradle and cover were to be manufactured using plastic injection molding, the size could be reduced. Additionally, the electronics can be arranged to be wearable, say in a fanny pack of sorts.

2. More dense material for the gyroscope: Increasing the effectiveness of the gyroscope comes at the cost of high angular velocity and mass. Brass was chosen for its density and ease of machinability for the device. However, using denser materials than brass is recommended because this can increase the effectiveness of the gyroscope without impacting the size of the disk.

3. Balancing of the gyroscope: One avenue of research not pursued due to its complexity was the dynamic balancing of the gyroscope. Balancing the gyroscope would reduce the vibration, as well as noise being generated within the system.

4. Incorporate more sensing equipment and code: The team considered having the prototype be smart sensing. Using an array of sensors such as the accelerometer and gyroscope, the idea was to create a self-sensing device that when a tremor was detected, would adjust the motor RPM accordingly. A combination of an Arduino and Raspberry PI was considered to allow for interconnectivity between the sensors and the PI to store the sensor data and return a signal to

adjust the motor speed. Research had been done to study the relationship between levels of tremor and transducer readings, however due to the complexity of this feature, it was dropped.

5. <u>Improve hand attachment mechanism:</u> The team would like to recommend improving the comfort of the device by constructing a new hand attachment mechanism. The 3D printed mount plate allows a customization to a variety of hand sizes, yet the attachment method of Velcro straps had room for improvement. The team considered the possibility of using a fingerless glove and the mount would be either glued, sewn or slotted into the glove.

6. <u>Hand tremor simulation:</u> In testing the device, the team brainstormed an alternative experiment that would simulate a tremor on a test platform. As discussed above in Section 6.5, the team was unable to successful build and conduct this test. However, the team believes that this test would be the next step in determining the effectiveness of the prototype.

Overall, the prototype proved to be successful in both theory and practice. The device comfortably fits on a hand and reduces the magnitude of hand tremors. As can be seen in our results, testing demonstrated an 80% reduction in tremors. The team believes that further testing with the tremor simulation device outlined above has the potential to yield more enlightening results. From the mathematical model, we concluded that our design is theoretically capable of increasing the reduction in tremors up to 87%.

WORKS CITED

Allen, Brendon Connor. "Effect of Gyroscope Parameters on Gyroscopic Tremor Suppression in a Single Degree of Freedom." Brigham Young University, 2018. Print.

APDA. "Tremor in Parkinson's." *American Parkinson Disease Association (APDA).* Web. Nov 12, 2018 <https://www.apdaparkinson.org/what-is-parkinsons/symptoms/tremor/>.

Arnon, Stephen S., et al. "Botulinum Toxin as a Biological Weapon: Medical and Public Health Management." *JAMA* 285.8 (2001): 1059-70. Web. Nov 20, 2018.

Britannica. "Cerebellum." *Encyclopaedia Britannica.* Web. Nov 12, 2018 <https://www.britannica.com/science/cerebellum>.

"Brotherhobby Returner R3 2207 2550kv Brushless Motor." *getfpv.com.* Web. Dec 14, 2018 <https://www.getfpv.com/brotherhobby-returner-r3-2207-2550kv-brushless-motor.html?gclid=Cj0KCQiAxs3gBRDGARIsAO4tqq2F7kjW_5LxBgdEc12poV4A_KejaYzYNbTCacM-Rdlb7TczZ2ofZcEaApYsEALw_wcB>.

Brozek, J. L., et al. "Original Article." *Allergy* 63.1 (2008): 38. *Toxicology Abstracts.* Web.

Burblla, L. F., et al. "The Science of Parkinson's." Sept 7, 2017. Web. Dec 10, 2018 <https://scienceofparkinsons.com/tag/l-dopa/>.

Burke, Deborah A., Robert A. Hauser, and Theresa A. McClain. "Essential Tremor." *Medscape.* Oct 22, 2018. Web. 12/6/2018 <https://emedicine.medscape.com/article/1150290-overview>.

Business Industry Reports. "World Deep Brain Stimulation Market Double Digit Growth Rate Forecasts To 2025." *Medium.com.* Dec 10, 2017. Web. Dec 14, 2018 <https://medium.com/@Precisemarketre/world-deep-brain-stimulation-market-double-digit-growth-rate-forecasts-to-2025-a196c37aa357>.

Calzetti, Stefano, et al. "Frequency/Amplitude Characteristics of Postural Tremor of the Hands in a

      Population of Patients with Bilateral Essential Tremor: Implications for the Classification and

      Mechanism of Essential Tremor." *Journal of Neurology, Neurosurgery & Psychiatry*

      (1987)Web.

Crawford, Paul, and Ethan E. Zimmerman. "Differentiation and Diagnosis of Tremor." *American*

      Academy of Family Physicians (AAFP). Mar 15, 2011. Web. Nov 11, 2018

      <https://www.aafp.org/afp/2011/0315/p697.html>.

Deuschl, Günther, et al. "A Randomized Trial of Deep-Brain Stimulation for Parkinson's Disease."

      New England Journal of Medicine 355.9 (2006): 896-908. Web. Nov 28, 2018.

"Drug Treatments for Essential Tremor." *WebMD.* Web. Nov 20, 2018

      <https://www.webmd.com/epilepsy/guide/essential-tremor-drug>.

"Eatwell Assistive Tableware Set." Web. December 4, 2018 <https://www.eatwellset.com/product-

      page/copy-of-8-piece-eatwell-assistive-tableware-set>.

Elble, Rodger J., and James McNames. "Using Portable Transducers to Measure Tremor Severity."

      (2016)Web.

Elble, Rodger J., Ludy Shih, and Jeffrey W. Cozzens. "Surgical Treatments for Essential Tremor."

      Expert Review of Neurotherapeutics 18.4 (2018): 303-21. Web. Dec 4, 2018.

Elble, Rodger J. "Defining Dystonic Tremor." *PMC* (2012)Web.

Elias, W. Jeffrey, et al. "A Randomized Trial of Focused Ultrasound Thalamotomy for Essential

      Tremor." *The New England Journal of Medicine* 375.8 (2016): 730-9. Web. Dec 2, 2018.

Essential Tremor: Common Medications.Web. Nov 26, 2018.

"GyroGlove." Web. 12/4/18 <https://gyrogear.co/gyroglove>.

Healthwise Staff. "Thalamotomy for Parkinson's Disease." *UW Health.* Oct 9, 2017. Web. Nov 20,

    2018 <https://www.uwhealth.org/health/topic/surgicaldetail/thalamotomy-for-parkinson-s-

    disease/aa140809.html>.

Hedera, Peter. "What Is the Best Treatment for Essential Tremor?" *MDedge.* Nov 23, 2015. Web.

    Nov 28, 2018 <https://www.mdedge.com/neurologyreviews/article/104128/movement-

    disorders/what-best-treatment-essential-tremor>.

Jankovic, Joseph, and NORD. "Primary Orthostatic Tremor." *National Organization for Rare*

    Diseases (Nord). 2017. Web. Nov 12, 2018 <https://rarediseases.org/rare-diseases/primary-

    orthostatic-tremor/>.

Joseph, J. P., and K. Rajappan. "Radiofrequency Ablation of Cardiac Arrhythmias: Past, Present and

    Future." (2012)Web.

Jung, Na Young, and Jin Woo Chang. "Magnetic Resonance-Guided Focused Ultrasound in

    Neurosurgery: Taking Lessons from the Past to Inform the Future." *Journal of Korean*

    Medical Science 33.44 (2018)*CrossRef.* Web.

"Keatlery Weighted Utensils." Web. December 4, 2018 <http://www.elderstore.net/keatlery.aspx>.

Kent, Michael. *The Oxford Dictionary of Sports Science & Medicine.* 3rd ed. Oxford University

    Press, 2016. Print.

"Liftware Steady." Web. December 4, 2018 <https://www.liftware.com/steady/>.

Mayo Clinic. "Parkinson's Disease." *Mayo Clinic.* Jun 30, 2018. Web. Nov 12, 2018

    <https://www.mayoclinic.org/diseases-conditions/parkinsons-disease/symptoms-causes/syc-

    20376055>.

Niemann, Nicki, and Joseph Jankovic. "Botulinum Toxin for the Treatment of Hand Tremor." *Toxins*

    10.7 (2018): 299. *PubMed.* Web.

NINDS, and National Institutes of Health. "Tremor Fact Sheet." *National Institute of Neurological Disorders and Stroke (NINDS).* May, 2017. Web. Nov 11, 2018 <https://www.ninds.nih.gov/Disorders/Patient-Caregiver-Education/Fact-Sheets/Tremor-Fact-Sheet>.

Parkin, Simon. "Hope in a Glove for Parkinson's Patients." *Technologyreviews.com.* Jan 14, 2016. Web. <https://www.technologyreview.com/s/545456/hope-in-a-glove-for-parkinsons-patients/>.

"Readi Steadi." 2016. Web. December 4, 2018 <https://www.readi-steadi.com/details.html>.

"Rocker Knife with T-handle." Web. December 4, 2018 <https://www.caregiverproducts.com/rocker-knife-t-handle.html>.

"S'up Spoon Black." *Sup-products.com.* Web. December 4, 2018 <https://www.sup-products.com/product/sup-spoon-black/>.

Salat, David, and Eduardo Tolosa. "Levodopa in the Treatment of Parkinson's Disease: Current Status and New Developments." *Journal of Parkinson's disease* 3.3 (2013): 255. *MEDLINE.* Web.

"Steadiwear." 2018. Web. <https://www.steadiwear.com/>.

"SteadyRest." 2016. Web. December 4, 2018 <https://www.steadyrest.org/>.

"Turnigy 5000mAh 5S 30C Lipo Pack w/XT-90." *HobbyKing.* Web. Dec 14, 2018 <https://hobbyking.com/en_us/turnigy-5000mah-5s-30c-lipo-pack-xt-90.html>.

"YEP 60A (2~6S) SBEC Brushless Speed Controller." *HobbyKing.* Web. Dec 14, 2018 <https://hobbyking.com/en_us/hobbyking-yep-60a-2-6s-sbec-brushless-speed-controller.html>.

APPENDIX A: THERMAL EXPANSION CALCULATIONS FOR SHRINK FIT

TABLE 2: NOMENCLATURE FOR THERMAL EXPANSION CALCULATIONS

Variable	Units
D = Distance	Millimeters
T = Temperature	Degrees Celsius
α = Thermal Conductivity	$10^{-6}{}^{\circ}C$

Calculation Parameters:

These calculations will be based off of 3 scenarios: Worst case, Measured Case, and Best Case. The worst case displays what will happen if the reaming tool is exactly 4.93mm (or 4.95mm) and the shaft is on the highest end of its tolerance. Measured case will display what will happen if the items are the actual size they were measured to and in the case of the reamer being 4.93mm (or 4.95mm). The best case will be if the shaft diameter is at the low side of the tolerance and the reaming tool is oversized. For purposes of the design, the worst-case scenario will be the basis the design.

Given:

Variables/Values	Description/Reasoning
$D_{meas} = 4.963\ mm$	The expected diameter of the shaft
$D_{max} = 4.964\ mm$	The diameter on the upper end of the tolerance
$D_{best} = 4.962\ mm$	The diameter on the lower end of the tolerance
$T_1 = 21{}^{\circ}C$	Room temperature

$T_2 = 260°C$	Max temperature of a standard oven
$D_{meas.diff}$	Difference in diameter between the shaft and hole with expected diameter at given diameters
$D_{max.diff}$	Difference in diameter between the shaft and hole with upper end of tolerance
$D_{best.diff}$	Difference in diameter between the shaft and the hole with lower end of the tolerance
$D_{meas.diff.cold}$	Difference in diameter between the shaft and hole with expected diameter with cold shaft
$D_{max.diff.cold}$	Difference in diameter between the shaft and hole with upper end of the tolerance with a cold shaft
$D_{best.diff.cold}$	Difference in diameter between the shaft and the hole with lower end of the tolerance with a cold shaft

Calculations:

Function	Result
Difference in diameter between the shaft and shaft hole $D_{final} = D_{initial}[1 + \alpha(T_2 - T_1)]$	$D_{meas.diff} = .0075mm$ $D_{max.diff} = .00922mm$ $D_{best.diff} = .015mm$ $D_{meas.diff.cold} = .012mm$ $D_{max.diff.colds} = .01mm$ $D_{best.diff.cold} = .018mm$

APPENDIX B: INTERFERENCE STRESS AND FLYWHEEL HOOP STRESS

TABLE 3: NOMENCLATURE FOR STRESS CALCULATIONS

Variable	Units	Variable	Units
E = Young's Modulus	GPa	r = radius	Millimeters
μ = **Poisson's Ratio**	*(unitless)*	$\delta_r = radial\ interference$	Millimeters
p = pressure	MPa	σ = stress	MPa
D = diameter	Millimeters	δ =strain	Millimeters

Given:

Variables/Values	Description/Reasoning
$E_{brass} = 105\ GPa$	Young's Modulus of Brass
$E_{alum} = 69\ GPa$	Young's Modulus of Aluminum 7075
$\mu_{brass} = 0.34$	Poisson's Ratio of Brass
$\mu_{alum} = 0.33$	Poisson's Ratio of Aluminum 7075
$\delta_r = 0.00795mm$	Radial Interference between gyroscope bore and shaft
$r_i = 0$	Inner radius of hollow shaft. 0 for solid shaft.
$D_{shaftmax} = 4.96443\ mm$	Maximum shaft diameter
$D_{boremin} = 2.480945\ mm$	Minimum gyroscope bore diameter

Calculations:

Function	Result
Radial Interference: $$\delta_r = \frac{D_{shaftmax}}{2} - \frac{D_{boremin}}{2}$$	$\delta_r = 0.00127\text{mm}$
Pressure between the gyroscope bore and shaft: $$p = \frac{\delta_r}{\frac{r_{shaft}}{E_{brass}} \cdot \left(\frac{r_{bore}^2 + r_{shaft}^2}{r_{bore}^2 - r_{shaft}^2} + \mu_{brass}\right) + \frac{r_{shaft}}{E_{alum}} \cdot \left(\frac{r_{shaft}^2 + r_i^2}{r_{shaft}^2 - r_i^2} + \mu_{alum}\right)}$$	$p = -0.028\text{ MPa}$
Stress on gyroscope bore (Tension): $$\sigma_{disk} = p \cdot \left(\frac{r_{bore}^2 + r_{shaft}^2}{r_{bore}^2 - r_{shaft}^2}\right)$$	$\sigma_{disk} = 53.76\text{ MPa}$
Stress on shaft (Compression): $$\sigma_{disk} = -p$$	$\sigma_{shaft} = 0.028\text{ MPa}$
Strain on gyroscope bore: $$\delta_{disk} = \frac{p \cdot r_{shaft}}{E_{brass}} \cdot \left(\frac{r_{bore}^2 + r_{shaft}^2}{r_{bore}^2 - r_{shaft}^2} + \mu_{brass}\right)$$	$\delta_{disk} = 0.001271\text{ mm}$
Strain on shaft: $$\delta_{shaft} = \frac{-p \cdot r_{shaft}}{E_{alum}} \cdot \left(\frac{r_{shaft}^2 + r_i^2}{r_{shaft}^2 - r_i^2} + \mu_{alum}\right)$$	$\delta_{shaft} = 6.6 * 10^{-7}\text{ mm}$

APPENDIX C: SHRINK FIT PROCESS

The gyroscope disk is uniformly heated in a convection oven to a temperature of 260 C (500 F) for at least two hours. At the same time, the motor shaft is cooled in a freezer to at least below 0 C (32 F). A plastic bag with a desiccant is used to contain the motor to prevent moisture from entering the internal windings. Two tubes of 1 in aluminum tubing in parallel act as a platform. Aluminum is used because it is a low-cost sturdy material. The objective is to insert the motor shaft into the bore, rather than vice versa. The reason behind this is it is easier to control the assembly with a lighter component than hold a hot brass disk. Once the hot disk is removed from the oven, it is inverted and placed on top of the aluminum tubing as shown in Figure 44.
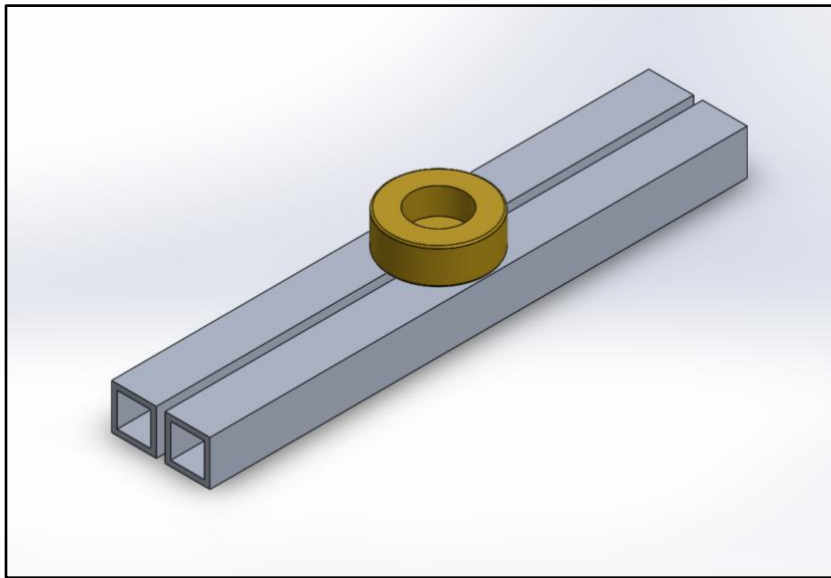

FIGURE 44: ALUMINUM TUBES SUPPORTING THE BRASS GYROSCOPE DISK

The bore is aligned with the spacing between the tubing and the cavity of the disk faces up as shown in Figure 45.
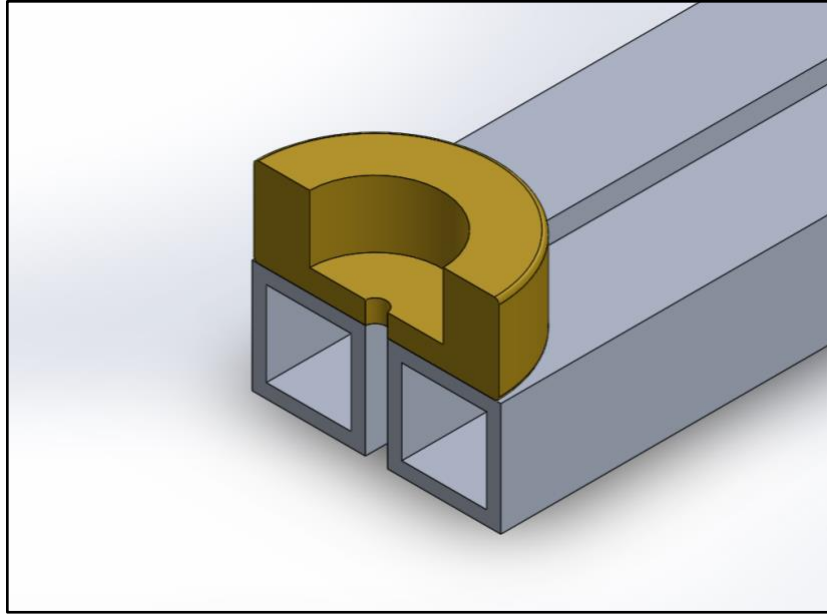
FIGURE 45:CROSS SECTION OF THE DISK PLACEMENT

The spacing between the tubing is equal if not larger than the diameter of the shaft. Therefore, when the shaft is inserted, the shaft will not contact the platform. The motor is removed from the freezer and mounted to a platform using screws. This platform is be maneuverable as once the motor is mounted, the platform will be held upside down. The bore and the shafts are aligned and holding the inverted motor platform, the interference is made by pushing the motor shaft down into the bore as positioned in Figure 46 and completed in Figure 47.
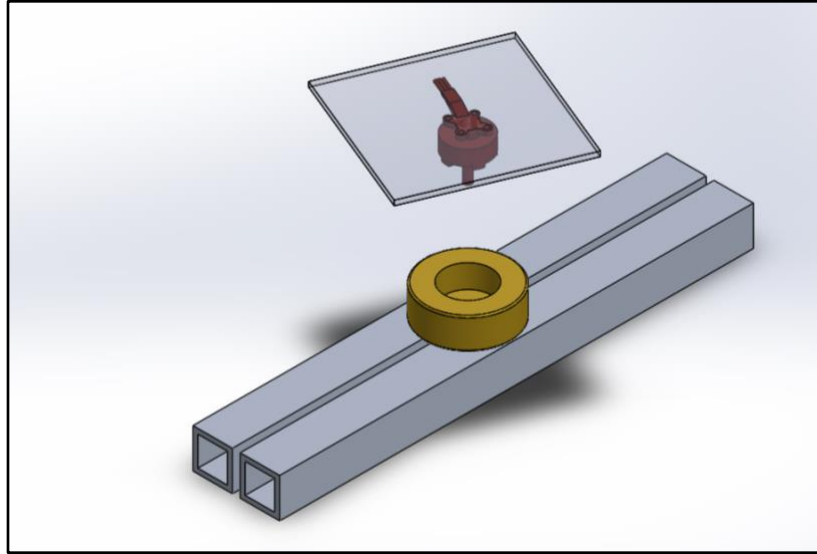
FIGURE 46: MOTOR SCREWED TO A PLATE AND ALIGNED WITH THE DISK BORE
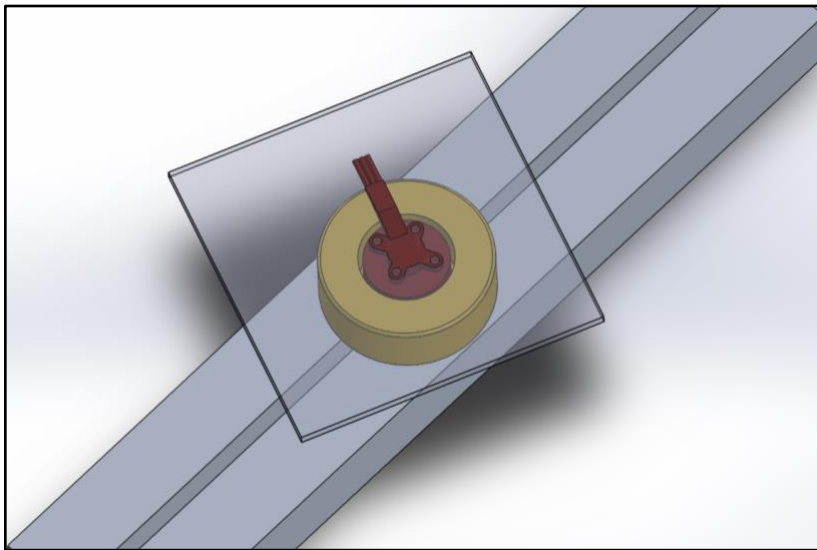
FIGURE 47: MOTOR SHAFT INSERTED INTO THE DISK BORE

Figure 48 shows the cross section of the complete assembly. Should there be resistance, the motor platform is lightly tapped down until the shaft is completely in. There may be some steam and smoke during contact, possibly due to the coating on the motor. Ideally, levels should be used on the aluminum platform and the motor platform to ensure the disk is axially aligned to the shaft and not at an angle. Once the shaft is in its desired position, the assembly is let to

acclimate to room temperature, or is safe to touch. The disk has been successfully mounted to the

shaft.

FIGURE 48: CROSS SECTION DEPICTING THE COMPLETE ASSEMBLY

APPENDIX D: LEVER ARM TEST PROCEDURE

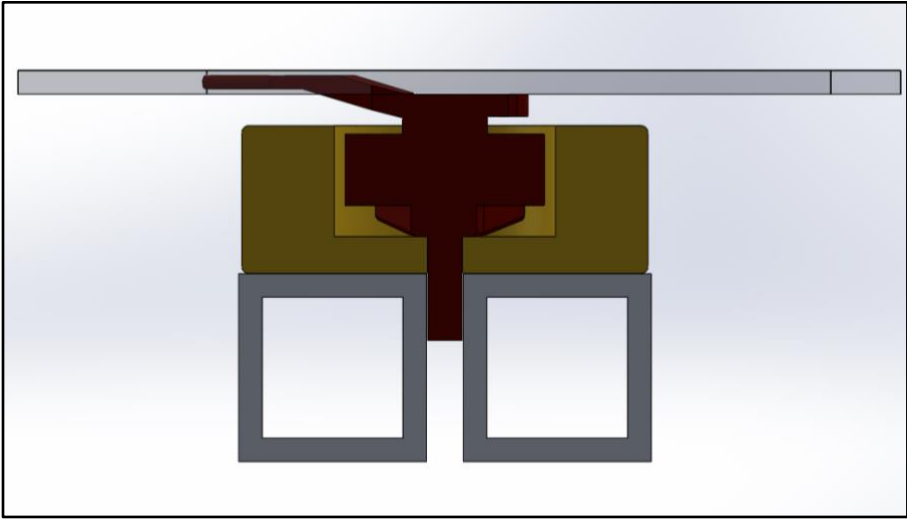The theory behind this test is that a gyroscope has resistance to its changes in motion. By mounting the gyroscope to a pivoting lever arm or pendulum, we can analyze the changes in motion caused by the gyroscope at different angular speeds. This test requires a test contraption that allows for the gyroscope assembly to be attached to a pendulum.

Required Materials:
- Pendulum Rig
- Gyroscope Prototype
- GoPro 7 (High Speed Camera)
- DSC-4783 Tripod
- Adobe Premiere Pro
- Poster with Marked Angles of Rotation

Setup:
1. Attach the gyroscope hand assembly to the end of the lever arm.
2. Position poster behind the pendulum and sketch angles of rotation for visualization
3. Set camera to record at 240 frames per second (fps)

Procedure:
1. Position the pendulum at a 5 degrees with the gyroscope turned off.
2. Record the rotation of the pendulum with the camera.
3. After the pendulum swings, stop the recording.
4. Repeat steps 1-3, running different trials with different angles, the gyroscope at various motor speeds with at least 3 trials per each change in independent variable.
   - Angles 5, 10, 15, 20 degrees
   - Effect of gyroscope enabled on pendulum, disabled on pendulum
     i. 6000 rpm
     ii. 10000 rpm
     iii. 14000 rpm
     iv. 18000 rpm
5. Compile this data in a spreadsheet and create a relationship of "Swing Time of the Pendulum as a Function of Motor RPM"
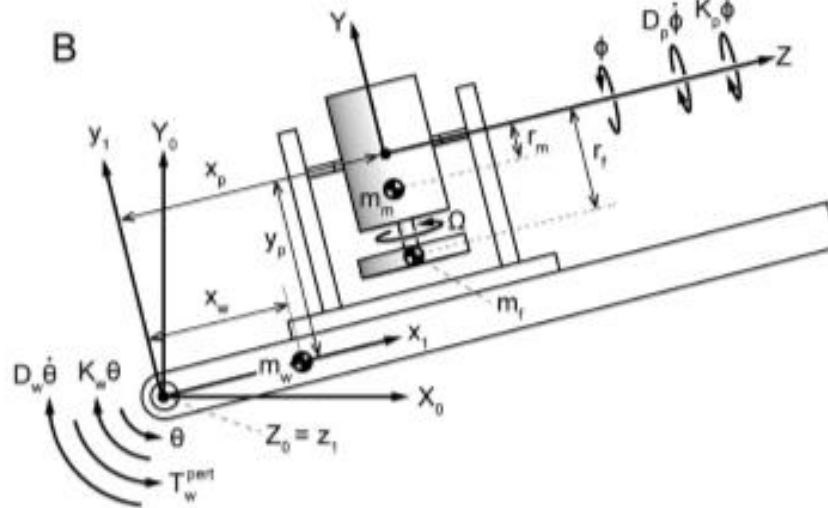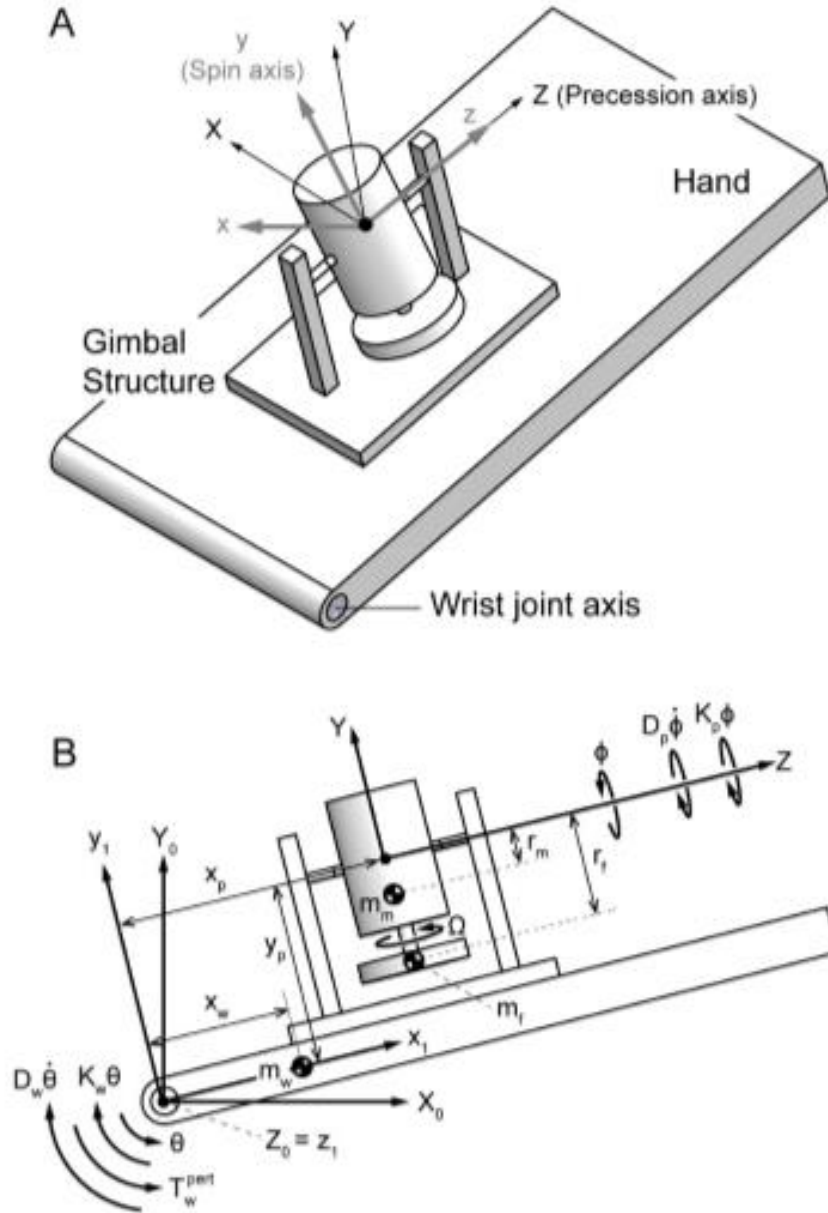
Lever Arm Test Calculations

Nomenclature:

Definition of Gravity: $G := g$ *Definition of a gram:* $g := \dfrac{1}{1000} kg$

Angular Dispisplacement About Pivot Pin: $\theta := 5deg$

Angular Velocity of Gyroscope $\Omega := 10000 rpm$

Angular Dispisplacement About Precession Axis: $\phi := 90deg$

Mass of the Gyroscope: $m_f := 196.47g$

Center of Precession Axis Along X1: $x_p := 482mm$

Center of Precession Axis Along Y1: $y_p := (38.5 + 25.4)mm$

COM of Gyroscope Along Y: $r_f := 5mm$

Gyroscope Moment of Inertia About X: $I_{xf} := 36525.22 g \cdot mm^2$

Gyroscope Moment of Inertia About Y: $I_{yf} := 60069.65 g \cdot mm^2$

Gyroscope Moment of Inertia About Y: $I_{zf} := 36525.22 g \cdot mm^2$

Mass of Lever $m_w := 141g$

COM of Lever Along X1: $x_w := \dfrac{514}{2} mm = 257 \cdot mm$

Mass of Lever: $m_L := 141g$

Mass of Device: $m_D := 460g$

Lever Length: $L_L := 514mm$

Dist. of Device: $L_D := 482mm$

COM: *Distance of the Center of Mass of the lever arm assembly from the pivot point.*

$$L := \frac{m_L \cdot \left(\frac{L_L}{2}\right) + m_D \cdot L_D}{m_L + m_D} \qquad\qquad L = 0.429\,m$$

Base Time: *Time for pendulum system to fall without the gyroscope spinning, assuming small angle.*

$$t_{cycle} := 2 \cdot \pi \cdot \sqrt{\frac{L}{G}} = 1.314\,s$$

$$t_{base} := \frac{t_{cycle}}{4} = 0.329\,s \qquad\qquad \textbf{Note:} \textit{ The cycle time is divided by 4 because the 90 deg. swing only represents a forth of its full motion.}$$

Moment of Inertia: *Inertias of Lever, Device and then combined for a total*

$$I_{beam} := \frac{1}{3} \cdot m_L \cdot L_L^2 = 0.012\,kg\cdot m^2 \qquad\qquad I_{device} := m_D \cdot L_D^2 = 0.107\,kg\cdot m^2$$

$$I_{zw} := I_{beam} + I_{device} \qquad\qquad I_{zw} = 0.119 \cdot kg\cdot m^2$$

Input Torue: *The amount of input torque caused by gravity.*

$$\theta = \theta_0 + \frac{1}{2} \cdot \alpha \cdot t^2 \qquad\qquad \alpha := \frac{2 \cdot \theta}{t_{base}^2} = 92.599 \cdot \frac{deg}{s^2}$$

$$T_{w.in} := I_{zw} \cdot \alpha = 0.193 \cdot N \cdot m$$

Angular Velocity About the Wrist Joint: $\qquad\qquad \omega := \frac{\theta}{t_{base}} = 15.215 \cdot \frac{deg}{sec}$

Angular Velocity About the Precession Axis: $\qquad\qquad \varphi := \frac{T_{w.in}}{I_{yf} \cdot \Omega} = 175.596 \cdot \frac{deg}{sec}$

Angular Acceleration of the Hand and Precession Movements:

$$q := \begin{pmatrix} \theta \\ \phi \end{pmatrix} = \begin{pmatrix} 5 \\ 90 \end{pmatrix} \cdot deg \qquad\qquad q_{acc} := \begin{pmatrix} \dfrac{T_{w.in}}{I_{zw}} \\ \dfrac{\varphi}{t_{base}} \end{pmatrix} = \begin{pmatrix} 92.599 \\ 534.341 \end{pmatrix} \cdot \frac{deg}{s^2}$$

Torques About the Hand and Precession Axis:

$$F = \begin{pmatrix} T_{w.r} + T_{w.in} \\ T_p \end{pmatrix}$$

NOTE:
T.w.r is the reactionary torque caused by the system.
T.p is the torque generated about the precession axis.

Moment of Inertia Components of the Gyroscope:

$$H := \begin{pmatrix} m_f \cdot x_p^2 + m_f \cdot y_p^2 + m_f \cdot r_f^2 \cdot \cos(\phi)^2 + 2 \cdot m_f \cdot y_p \cdot r_f \cdot \cos(\phi) + I_{xf} \cdot \cos(\phi)^2 \ldots & -m_f \cdot x_p \cdot r_f \cdot \sin(\phi) \\ + I_{yf} \cdot \sin(\phi)^2 + m_w \cdot x_w^2 + I_{zw} + m_f \cdot x_p \cdot r_f \cdot \sin(\phi) & \\ -m_f \cdot x_p \cdot r_f \cdot \sin(\phi) & m_f \cdot r_f^2 + I_{zf} \end{pmatrix}$$

Torques Based of the Moment of Inertias and Movements of the System:

$$C := \begin{pmatrix} -2 \cdot m_f \cdot \omega \cdot \varphi \cdot r_f^2 \cdot \cos(\phi) \cdot \sin(\phi) - 2 \cdot m_f \cdot y_p \cdot r_f \cdot \omega \cdot \varphi \cdot \sin(\phi) - 2 \cdot I_{xf} \cdot \omega \cdot \varphi \cdot \cos(\phi) \cdot \sin(\phi) \ldots \\ + I_{yf} \cdot \Omega \cdot \varphi \cdot \cos(\phi) + m_f \cdot G \cdot x_p \cdot \cos(\theta) - m_f \cdot G \cdot y_p \cdot \sin(\theta) + m_w \cdot G \cdot x_w \cdot \cos(\theta) \ldots \\ + -m_f \cdot G \cdot r_f \cdot \cos(\phi) \cdot \sin(\phi) - m_f \cdot x_p \cdot r_f \cdot \varphi^2 \cdot \cos(\phi) + 2 \cdot I_{yf} \cdot \omega \cdot \varphi \cdot \sin(\phi) \cdot \cos(\phi) \\ \\ m_f \cdot \omega^2 \cdot r_f^2 \cdot \cos(\phi) \cdot \sin(\phi) - I_{yf} \cdot \omega^2 \cdot \sin(\phi) \cdot \cos(\phi) + I_{xf} \cdot \omega^2 \cdot \cos(\phi) \cdot \sin(\phi) \ldots \\ + m_f \cdot y_p \cdot r_f \cdot \omega^2 \cdot \sin(\phi) - I_{yf} \cdot \Omega \cdot \omega \cdot \cos(\phi) - m_f \cdot G \cdot r_f \cdot \sin(\phi) \end{pmatrix}$$

Equilibrium Torues:

$$F = H \cdot q_{acc} + C$$

$$\begin{pmatrix} T_{w.r} \\ T_p \end{pmatrix} := H \cdot q_{acc} + C - \begin{pmatrix} T_{w.in} \\ 0 \end{pmatrix} = \begin{pmatrix} 1.355 \\ -0.01 \end{pmatrix} \cdot N \cdot m$$

Based Off of These Conditions, the Realized Torque and Percentage of Reduction Are:

$$T_{realize} := T_{w.r} = 1.355 \cdot N \cdot m$$

$$Percent := \frac{T_{w.in}}{T_{realize}} = 0.142$$

$$Time_{realize} := t_{base} \cdot (1 + Percent) = 0.375 \, s$$

APPENDIX F: RPM TEST DATA

TABLE 4: RPM TEST DATA

PWM Width	RPM	PWM Width	RPM
875	4440	1275	14520
900	4680	1300	15480
925	5760	1325	15480
950	6000	1350	16200
975	7200	1375	16200
1000	8280	1400	16800
1025	8760	1425	17880
1050	9840	1450	17880
1075	10000	1475	18960
1100	11160	1500	18720
1125	12120	1525	19440
1150	12240	1550	20040
1175	12960	1575	20400
1200	12960	1600	2100
1225	13800	1625	21960
1250	13920	**2200**	**26400**

This table displays the data comparing the RPM of the motor read by the RPM sensor to the PWM reading on the servo tester.

APPENDIX G: LEVER ARM TEST DATA

TABLE 5: TEST DATA WITH 180 DEGREES OF CRADLE ROTATION

Gyroscope (RPM)	Angle (deg.)	Time (sec.)	Percent Increase
0		0.200	0
6000		0.302	50
10000	5	0.490	129
14000		0.234	16
18000		0.243	21
0		0.241	0
6000		0.339	41
10000	10	0.460	91
14000		0.250	4
18000		0.407	69
0		0.300	0
6000		0.329	10
10000	15	0.398	33
14000		0.291	3
18000		0.263	12

This table displays the lever arm test data with the cradle fully rotated to the right at the start of the swing.

Gyroscope (RPM)	Angle (deg.)	Time (sec.)	Percent Increase
0	5	0.201	0
6000		0.228	13
10000		0.292	56
14000		0.306	52
18000		0.491	144
0	10	0.241	0
6000		0.282	17
10000		0.313	30
14000		0.380	57
18000		0.441	83
0	15	0.300	0
6000		0.302	1
10000		0.346	15
14000		0.363	21
18000		0.413	38

This table displays the lever arm test data with the cradle located in the neutral position at the start of the swing.

APPENDIX H: SIMULATOR TEST PROCEDURE

This test aims to measure the reduction in tremor by artificially created a reproducible tremor. By measuring the before and after conditions with a gyroscopic sensor and accelerometer, the effectiveness of the device at reducing an artificially generated tremor can be computed. The importance of generating a tremor artificially is to keep the tremor experienced by the prototype constant and repeatable. To generate the tremor, a linear actuator is used to rotate a platform where the prototype is mounted. This also allows for different tremor amplitudes and frequencies to be applied to the prototype.

Required Materials:

- Linear Actuator
- Testing Rig (Shown Below)
- Power Source

- MPU 6050 (Gyroscope and Accelerometer)
- Arduino (Data Input)
- Gyroscope Prototype

Procedure without gyro glove prototype:

1. The armature is assembled with the dc motor and mass.
2. The dc motor is turned on and controlled to create an artificial tremor of a set amplitude and frequency.
3. Using a the MPU6050 transducer, data is gathered from the artificial tremor.

Procedure with gyro glove prototype:

4. The armature is assembled with the dc motor and mass and the gyro glove prototype
5. The dc motor is turned on and controlled to create the same artificial tremor of a set amplitude and frequency.
6. The gyro glove prototype is turned on at a set rpm to dampen the tremor.
7. Using a the MPU6050 transducer, data is gathered from the dampened artificial tremor.
8. The results are compared.

APPENDIX I: ARDUINO RPM CODE

Below is the script used for the Arduino Uno to read the signal from the RPM sensor and

display the measured speed of the gyroscope.

```
int encoder_pin = 2;  // The pin the encoder is connected
unsigned int rpm;      // rpm reading
volatile byte pulses;  // number of pulses
unsigned long timeold;
// The number of pulses per revolution
// depends on your index disc!! Use the number of holes on the encoder. For the reflective tape, use =1
unsigned int pulsesperturn = 1;

//Digital Smoothing variables
int sensVal=0;         // for raw sensor values
float filterVal;       // this determines smoothness  - .0001 is max  1 is off (no smoothing)
float smoothedVal;     // this holds the last loop value just use a unique variable for every different sensor
that needs smoothing

void counter()
{
  //Update count
  pulses++;

  int c = pulses%100;
  if (c==0) {
    Serial.print("   pulses = "); Serial.println(pulses);
  }
}

void setup()
{
  Serial.begin(9600);
  //Use statusPin to flash along with interrupts
  pinMode(encoder_pin, INPUT);

  //Interrupt 0 is digital pin 2, so that is where the IR detector is connected
  //Triggers onRPM FALLING (change from HIGH to LOW)
  attachInterrupt(0, counter, FALLING);
  // Initialize
  pulses = 0;
  rpm = 0;
  timeold = 0;

}

/*int smooth(int data, float filterVal, float smoothedVal2)
{
    if (filterVal > 1) { //check to make sure parameters are within range
```

```
     filterVal = 0.9999;
    }
    smoothedVal2=(data * (1 - filterVal)) + (smoothedVal2  * filterVal);
    return (int)smoothedVal2;
}*/

void loop()
{
//   Serial.print(" duration= "); Serial.println(millis() - timeold);

  if (millis() - timeold >= 1000) { /*Update in milliseconds, this will be equal to reading frecuency
(Hz).Do not change*/

    //Don't process interrupts during calculations
    detachInterrupt(0);
    //Note that this would be 60*1000/(millis() - timeold)*pulses if the interrupt
    //happened once per revolution
    rpm = (60000 / pulchesperturn ) / (millis() - timeold) * pulses;

    //Write it out to serial port
    Serial.print("RPM = ");
    Serial.print(rpm, DEC);
    Serial.print(" pulses= "); Serial.println(pulses);

    timeold = millis();
    pulses = 0;

    //Restart the interrupt processing
    attachInterrupt(0, counter, FALLING);
    //Serial.print("smoothedVal before ");
    //Serial.println(smoothedVal,DEC);

    sensVal = rpm;
    //smoothedVal = smooth(sensVal, filterVal, smoothedVal); //second parameter determines the
smoothness 0 is off 0.999 is max smooth

    //Serial.print(sensVal);
    //Serial.println("   ");
    //Serial.print(smoothedVal);
    //Serial.println("   ");
    //Serial.print("filterValue * 100 = ");
    //delay(30);
    //Serial.print("SmoothRPM = ");
    //Serial.println(smoothedVal, DEC);

  } // end of if
} // end of loop
```